Region II Storm Surge Project - Recurrence Interval Analysis of Coastal Storm Surge Levels and Wave Characteristics

September 2014

FEMA

Federal Emergency Management Agency
Department of Homeland Security
500 C Street, SW
Washington DC, 20472

Contract: HSFEHQ-09-D-0369
Task Order: HSFE02-09-J-0001

This document was prepared by

RAMPP
8401 Arlington Blvd.
Fairfax, VA 22031

Figures

Tables

ADCIRC	ADvanced CIRCulation Model for Oceanic, Coastal and Estuarine Waters
CDF	Cumulative Distribution Function
CCDF	Complementary Cumulative Density Function
cm	Centimeter
FEMA	Federal Emergency Management Agency
GEV	Generalized Extreme Value
HWM	High Water Mark
JPM	Joint Probability Method
km	Kilometer
m	Meter
NOAA	National Oceanic and Atmospheric Administration
PDF	Probability Density Function
QA/QC	Quality Assurance/Quality Control
RAMPP	Risk Assessment, Mapping, and Planning Partners
s	Second
SWAN	Simulating WAves Nearshore
TC	Tropical Cyclone
UnSWAN	Unstructured Version of SWAN model
WHAFIS	Wave Height Analysis for Flood Insurance Studies

SECTION ONE INTRODUCTION

The Federal Emergency Management Agency (FEMA) contracted Risk Assessment, Mapping, and Planning Partners (RAMPP), a joint venture of Dewberry, URS, and ESP, under its Risk Mapping, Assessment, and Planning (Risk MAP) program to provide comprehensive floodplain mapping, Geographic Information System (GIS), and hazard risk mitigation services. The results from the Region II storm surge model production simulations for the New Jersey and New York project area have been processed to develop recurrence interval stillwater elevations and wave characteristics. The processing was applied to determine the stillwater elevations for the 10-, 2-, 1- and 0.2-percent-annual-chance exceedance levels. Analysis was also performed to determine the significant wave height and peak wave period associated with the 1-percent-annual-chance exceedance level for application in the overland wave analysis. This report details the methods used and results of the recurrence interval analysis. The development of the recurrence interval stillwater elevations is discussed in Section Two, and the development of the wave characteristics is discussed in Section Three.

SECTION TWO A METHOD TO DETERMINE THE STILLWATER ELEVATIONS RESULTING FROM STORM SURGE IN THE NEW JERSEY AND NEW YORK PROJECT AREA

2.1 APPROACH

The calculation of the stillwater elevations for the 10-, 2-, 1- and 0.2-percent-annual-exceedance levels within the New Jersey and New York project area required separate treatment of tropical cyclones (TCs) and extratropical storms. The relative importance of storm surges in the project area resulting from extratropical storms such as Nor'easters is considerable compared to the surge elevations and frequencies associated with TCs. This is because TCs, especially those of hurricane strength, occur much less frequently than Nor'easters. TCs that affect the U.S. northeast coast are usually weakened by interactions with surrounding meteorological and oceanographic conditions. Accordingly, the storm surge elevations are noticeably lower than those of TCs affecting the Southeast and Gulf States.

As results from the modeling of the 30 strongest extratropical storms during a 60-year period of record became available, they demonstrated that extratropical storms are significant contributors to coastal flooding. Just as important, there were noticeable differences in the surge heights for individual storms over the entire study area. These findings prompted an evaluation of existing and potential methods for characterizing the annual occurrence probability distributions for surge elevations from extratropical storms across the study area.

The approach for combining the separate analysis of TCs and extratropical storms was to develop individual probability distributions for each of the two storm types and then combine them. The stillwater elevations for the 10-, 2-, 1- and 0.2-percent-annual-chance exceedance levels were then interpolated from the final combined cumulative distribution. Sections 2.2 and 2.3 describe the methods used to develop the stillwater elevation probability distributions for the extratropical storms and TCs. Section 2.4 describes the methods applied to develop the combined cumulative distributions.

2.2 METHODS APPLIED FOR EXTRATROPICAL STORMS

A simple way to display the general characteristics of surge elevations resulting from the 30 modeled extratropical storms is to plot the elevations against the relative rank of the computed surge elevation for selected points within the study area. Figure 1 shows the plots for six locations in Cape May County, New Jersey, which is located at the southern end of the project area's Atlantic shoreline. In this case, the surge heights increase relatively consistently with their rank, with values ranging between 1.0 meter (m) and 2.5 m.

In contrast, similar plots from six coastal points representing western Long Island Sound and the East River are shown in Figure 2. These surge values are noticeably greater than those in Figure 1. It is also clear that the relatively uniform increase in the surge elevation coinciding with increasing storm rank shown in Figure 1 is not characteristic of those shown on Figure 2. Instead, the two highest ranking points are considerably greater than the overall trend, followed by their lower ranking neighbors.

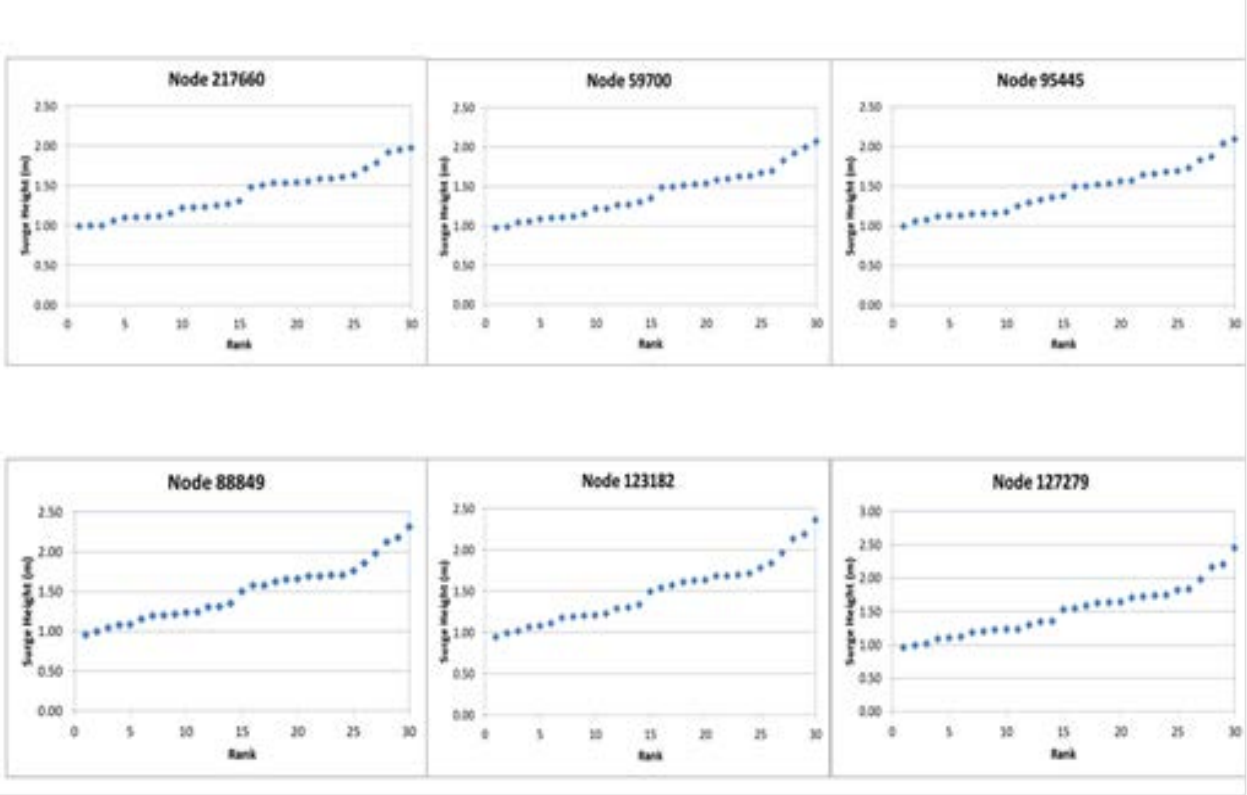

Figure 1. Surge elevation versus relative rank for six coastal points in Cape May County, NJ

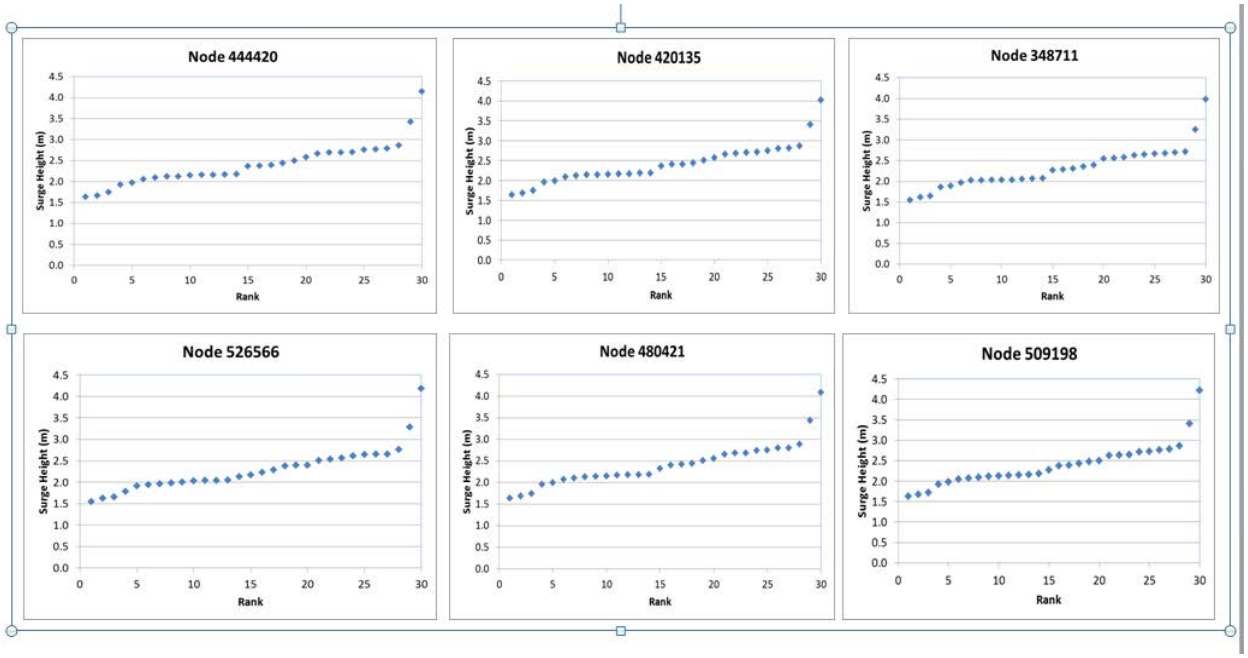

Figure 2. Surge elevation versus relative rank for six coastal points in western Long Island Sound and the East River

These two sets of example results illustrated a number of important characteristics:

- The magnitudes of the extratropical storm surges are comparable to those caused by TCs.
- The extratropical storm surges are different across the study area because of the local orientation of the shoreline; the geometries of the harbors, bays and sounds; and spatial gradients in the storm intensities over the large scale of the project area.
- In some cases, the patterns of storm surge elevations versus rank show a deviation from the overall trend, which may be the result of "sample variability[1]."

The patterns of the relative storm surge elevations are further complicated when overland flooding is considered. As the ground elevation increases farther inland from the shoreline, fewer of the individual storms cause flooding. This is illustrated in Figure 3. Point 13 is located in the tidal portion of the Mullica River, just west of Great Bay, where all 30 extratropical storms resulted in simulated surge elevations. Points 14, 15 and 16 are located at progressively higher land elevations, where fewer and fewer of the storms cause flooding. Therefore, the content and overall pattern of the surge height distribution is altered moving inland along these selected points.

The surge height distribution characteristics illustrated by Figures 1, 2, and 3 generated the following questions:

- What is an adequate representation of distributions that shows significant differences from place to place over the study area?
- What is an appropriate way to characterize the different shapes of the surge height distributions, paying special attention to places where seemingly anomalous surge height differences occur among the highest ranking events?
- How can the progressive decrease in the number of surge levels reaching inland points be appropriately characterized in evaluating the index annual exceedance surge elevations?

It was determined during the course of the study that a better representation of the tidal effects combined with the extratropical storm surge could be obtained by varying the tide phase with each of the storms. Consequently, each of the 30 extratropical storms was simulated twice to represent two different phases of the fortnightly tide cycle, yielding a total of 60 extratropical storm simulations.

2.2.1 Characterization of the Extratropical Surge Height Distributions

A variety of statistical functions has been used to characterize flood height distributions. These include the normal, log-normal, Gumbel, the Generalized Pareto, Weibul, Log-Pierson 3, and Generalized Extreme Value (GEV) distribution. Each distribution was tested for a representative set of points over the study area using the Kolmogorov-Smirnov, Andersen-Darling, and Chi-Squared goodness of fit tests. Using EASYFIT® software, the data were fit with a variety of distributions,

[1] Sample variation is a term for the inability to determine the exact value of a quantity using statistics because of limitations in the sample size. Considering node 509198 as an example, there are only two observations with surge above 3 m. As a result, considerable uncertainty exists in the proportion of storms in the overall population that exceed this value, and the observed proportion (2 out of 30) may or may not represent the proportion in the population. One way to illustrate this phenomenon is to consider that a very rare event, such as the 432-year surge, must occur during some given 60-year period. If it happened to be one of the two surge elevations, it would be attributed to an event with much higher frequency.

and then ranked by the goodness of fit tests. The results for each of the distributions commonly used in flood height analysis are shown in Table 1. The GEV distribution generally ranked highest among all three tests. The GEV distribution is frequently used to model natural extremes because of its asymptotic extreme-value properties and because of its flexibility. From this, it was concluded that the GEV distribution was an appropriate function to describe the probability distributions of the surge heights computed for the 30 extratropical storms in the analysis.

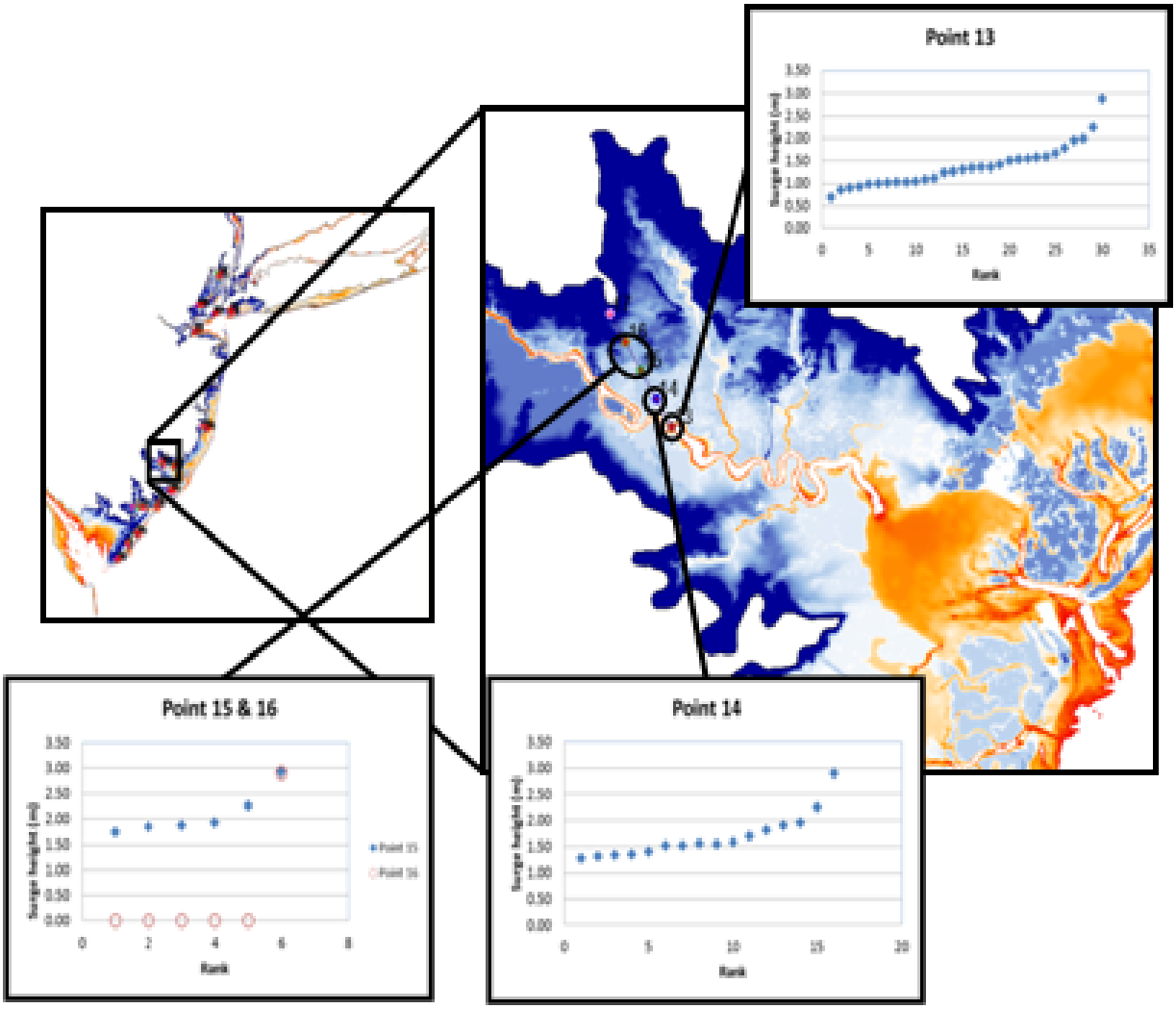

Figure 3. Surge elevation versus relative rank for example overland points

Table 1. Summary of Goodness of Fit Rankings

Distribution Type	*Average Rank*		
	Kolmogorov-Smirnov	*Anderson-Darling*	*Chi-Squared*
Gen. Extreme Value	7	3	10
Gen. Pareto	28	55	
Log-Pearson 3	12	8	16
Lognormal	18	19	15
Normal	37	40	37
Weibull	27	38	33

2.2.2 Use of the GEV Distribution

When the GEV distribution is determined for a point within the project area with a record of the full 60 computed surge heights (30 storms simulated twice), it is possible to directly determine its parameters using conventional methods (the L-Moment approach was used, but the method of maximum likelihood yields similar results). The resulting cumulative distribution function (CDF) can be characterized as $[X \leq x] = F_X(x; \mu, \sigma, \xi)$, where μ, σ, ξ are the three fitted parameters of the GEV distribution representing location, scale and shape of the distribution function, respectively.

The annual frequency of storms exceeding a surge value x is given by the complementary cumulative density function (CCDF), which is defined as:

$$\frac{N}{T}\{1 - F_X(x;\ \mu, \sigma, \xi)\}$$

Although 60 storms were simulated and the results were used to estimate F_X, the true storm rate of 30 storms in 60 years was used to determine the annual exceedance frequency because the historical number of extratropical storms must be preserved in the calculations. Thus, N = 30 and T = 60 in the above equation.

2.2.3 Spatial Distribution of Extratropical Surge Height Distributions

The GEV distribution was fitted to a large number of shoreline points[2] over the project area to determine whether there were systematic changes that could be used to simplify the surge level analysis. Figure 4 shows a number of GEV cumulative distribution functions for these points. The curves are color coded according to sub-areas. An expanded plot is given in Figure 5.

Figures 4, 5, and 6 reveal that the extratropical surge height distributions vary considerably over the project area. Some of the sub-areas, such as Long Island Sound and the East River (Orange), have very similar GEV functions for all sampled points. Others, such as the southern New Jersey coast (Red), also have well clustered distributions, but these change in a systematic manner with distance along the shoreline. A third behavior is illustrated by points within New York Harbor and adjacent places (Blue). In this area, the GEV functions change noticeably from point to point.

[2] Here the term *shoreline point(s)* is used when referring to model output points that are located offshore but close to the normal shoreline (Mean sea level). These output points have storm surge heights for all of the modeled extratropical storms.

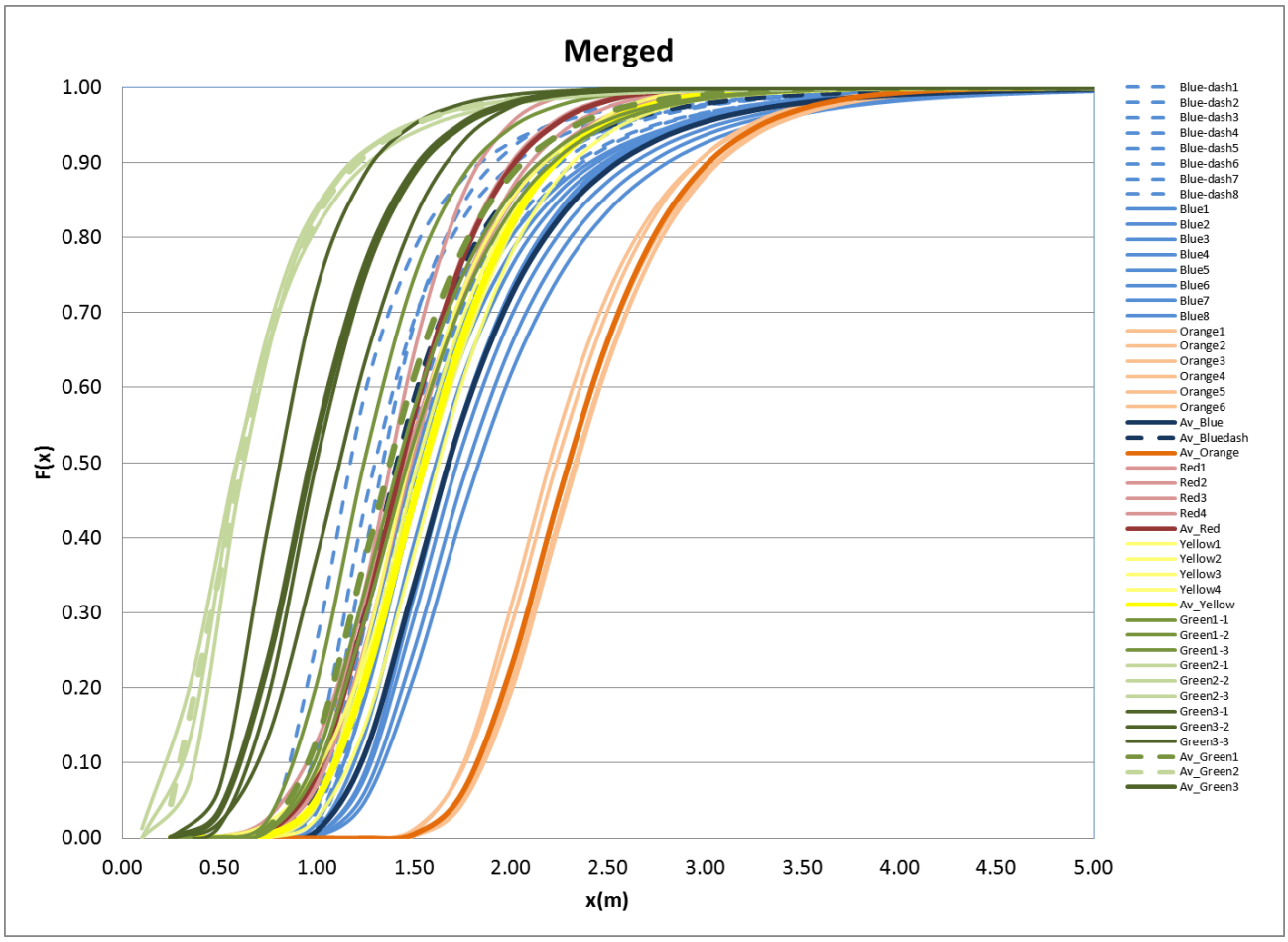

Figure 4. Cumulative distribution functions representing the computed surge heights at a number of points across the project area. Bold lines are composites for the sub-areas.

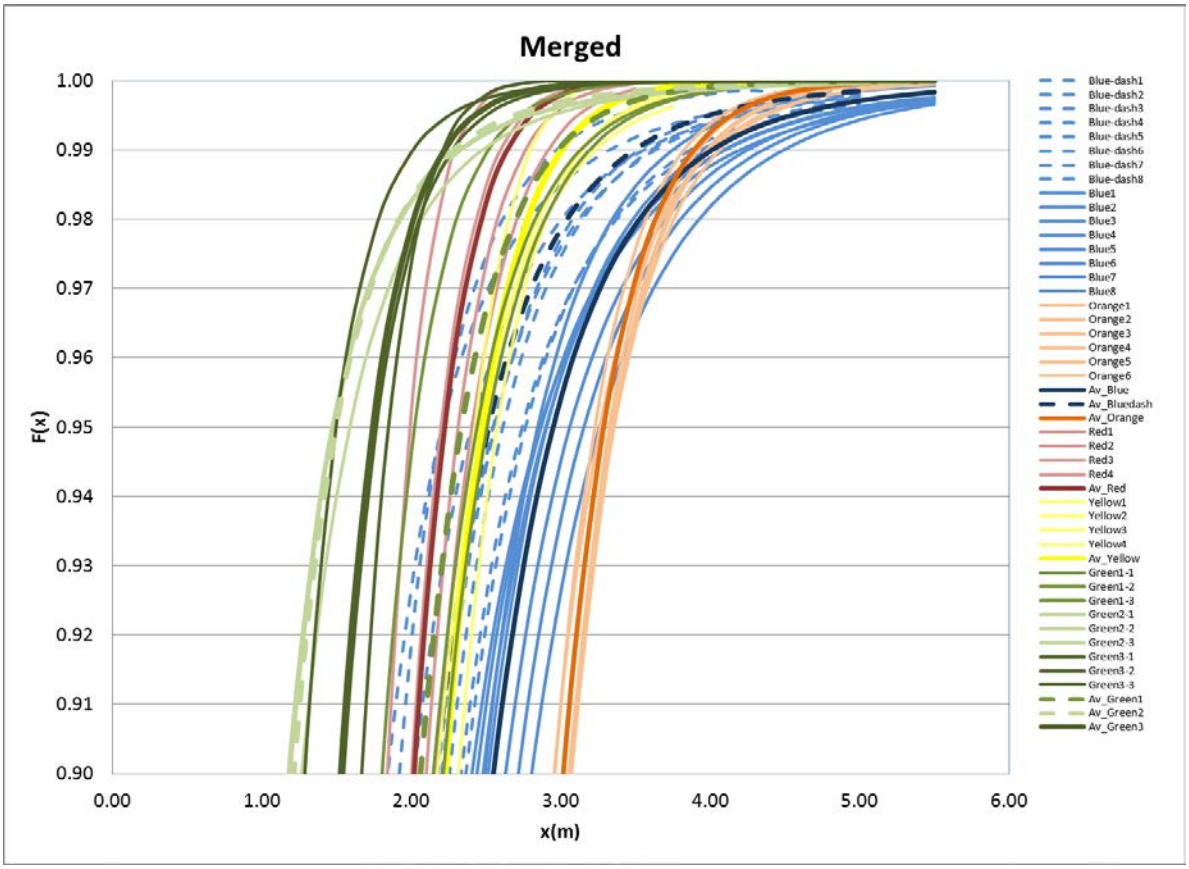

Figure 5. Expanded view of the upper cumulative probability values for the functions shown in Figure 4. Note that because there were actually 60 storms simulated in 60 years (30 storms simulated twice), the 0.01/year values are associated with the cumulative probability of 0.98.

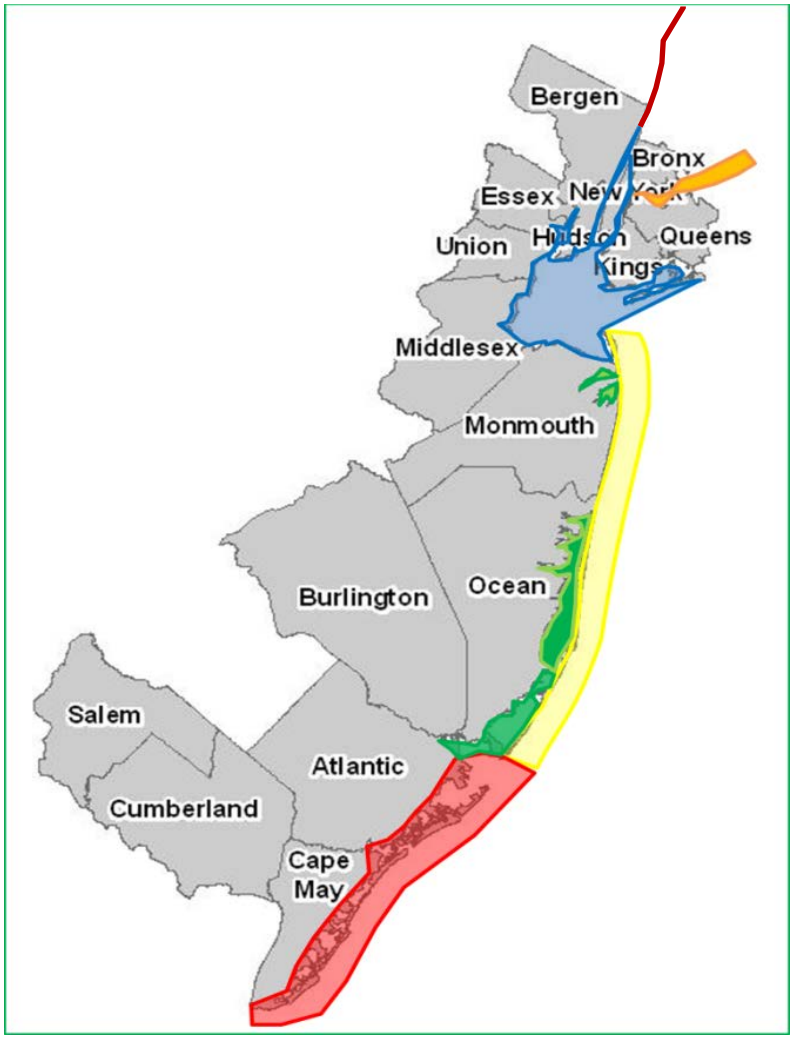

Figure 6. Sub-areas determined by similarities in the GEV functions of representative shoreline points with colors corresponding to the grouping shown in Figures 4 and 5

Overall, these results discouraged the attempt to develop an analysis method that relied on dividing the region into sub--areas. Instead, it appeared that a point-by-point fitting of the GEV distribution was needed.

2.2.4 Analysis of Inland Surge Elevations

Inland surge elevation analyses are different for extratropical events compared to TC events. The analysis of TCs is based on a parametric representation of the storm characteristics, and the exceedance frequency for a given surge level x is calculated by numerical integration. The numerical integration starts from the largest surge level downward and stops when the surge does not exceed the ground elevation. Thus, the absence of surge levels at inland points for the smaller storms does not impact the analysis. This is not the case for extratropical events because the entire set of surge elevations are fit as a group. This approach works well at offshore points when all events yield a non-zero surge elevation, but is problematic at inland points because the number of flooding events decreases as the land rises going inland.

Figure 7 illustrates the method used to fit GEV functions to points located inland from the normal shoreline. In Figure 7, points located in the ocean or coastal waterways have surge elevations for the full set of 60 extratropical storms that were simulated. Overland points have results from fewer flooding events as the land surface rises going inland. It is necessary to preserve the general characteristics of the GEV function for all 60 events to accurately determine the probability densities associated with the individual surge levels. In Figure 7, the probability density function (PDF) for the full set of 60 events at a shoreline point (Point C) is shown with a red fill. The probability densities associated with modeled surges that reach inland are shown with a light blue fill (Point B) and a dark blue fill (Point A). The number of these actual events is fewer than the full set seen at Point C. To fit the GEV function to the two inland points, the "missing" portion of the set of 60 events was "borrowed" from the nearest place where the full set of 60 was available. These "borrowed" probability densities are shown with red filled curves for Points A and B. Point A requires more borrowed values than B because its ground elevation is higher and it encounters fewer storm surges. The green line represents the GEV function that is fitted to this combined data set. The fitted curve departs from both the red and blue filled functions, but these departures are quite small.

This borrowing is justified by the fact that, for storms that produce non-zero surge at inland points, there is a very high correlation between the surge at the inland points and the surge at the coastal points closest to them (i.e., the maximum surge level surface is nearly flat).

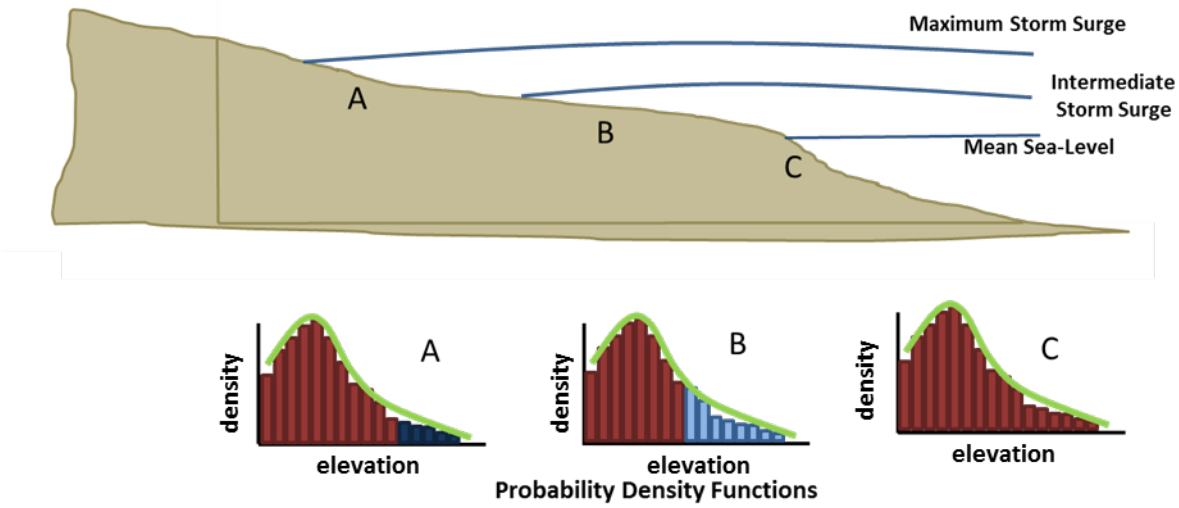

Figure 7. Schematic diagram illustrating the GEV function fitting procedure for flooded areas

The GEV approach was applied to each of the ADvanced CIRCulation Model (ADCIRC) nodes using the 60 storm outputs. The results of the GEV fit were then combined with the distributions obtained for the TC analysis. This approach provides detailed coverage of the combined impact of TCs and extratropical storms across the study area.

2.3 METHODS APPLIED FOR TROPICAL CYCLONES

2.3.1 Application of SURGE_STAT

The recurrence interval analysis was conducted using Version 1.1 of the utility software program SURGE_STAT developed by Fugro for the Federal Emergency Management Agency (FEMA) (Fugro William Lettis and Associates, Inc., 2009). The analysis requires the following information:

- A set of Joint Probability Method (JPM) points at which the flood elevations for each recurrence interval are calculated (the output points)
- Surge elevations for each storm at each output point
- Annual recurrence rates for each storm
- Standard deviations for the uncertainty terms

The number of JPM points and their spacing throughout the study area should be sufficient to provide smooth representation of the surge elevations over the area of interest. To make maximum use of the ADCIRC simulation results, all of the 604,790 ADCIRC nodes were used as JPM output points. This provided the maximum resolution and detailed coverage in the study area, and is consistent with the points used for the extratropical storm analysis. The surge elevations were obtained from the standard ADCIRC output files for each of the 159 storms, and the annual recurrence rates were obtained from the Joint Probability Analysis (RAMPP, 2014). An example of the maximum water elevation from a single storm event is shown in Figure 8.

The calculation method, implemented by the SURGE_STAT software program, is briefly described below and fully documented in the user's manual (Fugro William Lettis and Associates, Inc., 2009).

The method is applied individually to each JPM point. For each JPM point, a discrete histogram of the surge levels at each point is generated using 360 bins with an elevation width of 3 centimeters (cm), spanning the range from 0 to 11 m. The rate associated with each synthetic storm is accumulated into the appropriate bin. This process yields the total rate, Λ_j, where j is the bin index, which provides an approximation of the surge height annual-rate density function[3] at the point, similar to the example shown in Figure 9.

However, in order to account for uncertainty in the event simulations, each storm rate is spread over adjacent bins in the histogram.

Each bin's total rate Λ_j is calculated according to the following equation:

$$\Lambda_j^{new} = \sum_{i=1}^{360} \Lambda_i \alpha_i \, e^{-\frac{1}{2}\left[\frac{(x_i - x_j)}{\sigma_i}\right]^2} \qquad \text{Eq. 1}$$

where *j* is the index of a specific bin, *i* is the general index for all bins, *x* is the bin's center value, and α_i is a normalizing constant. The standard deviation σ_i represents the uncertainty in the numerical results and is bin-dependent. Details of the calculation of the uncertainty term are described in the next section.

The normalizing constant α_i ensures that the total event rates are conserved. It is necessary due to the discrete implementation of the Gaussian distribution. The normalizing constant is calculated as follows:

$$\alpha_i = \frac{1}{\sum_{k=1}^{360} e^{-\frac{1}{2}\left[\frac{(x_i - x_k)}{\sigma_i}\right]^2}} \qquad \text{Eq. 2}$$

[3] This is not a PDF because it does not integrate to unity. Instead, the rate Λ_j obtained for each bin is the annual rate of storms that cause the surge associated with that bin at the ADCIRC node being considered.

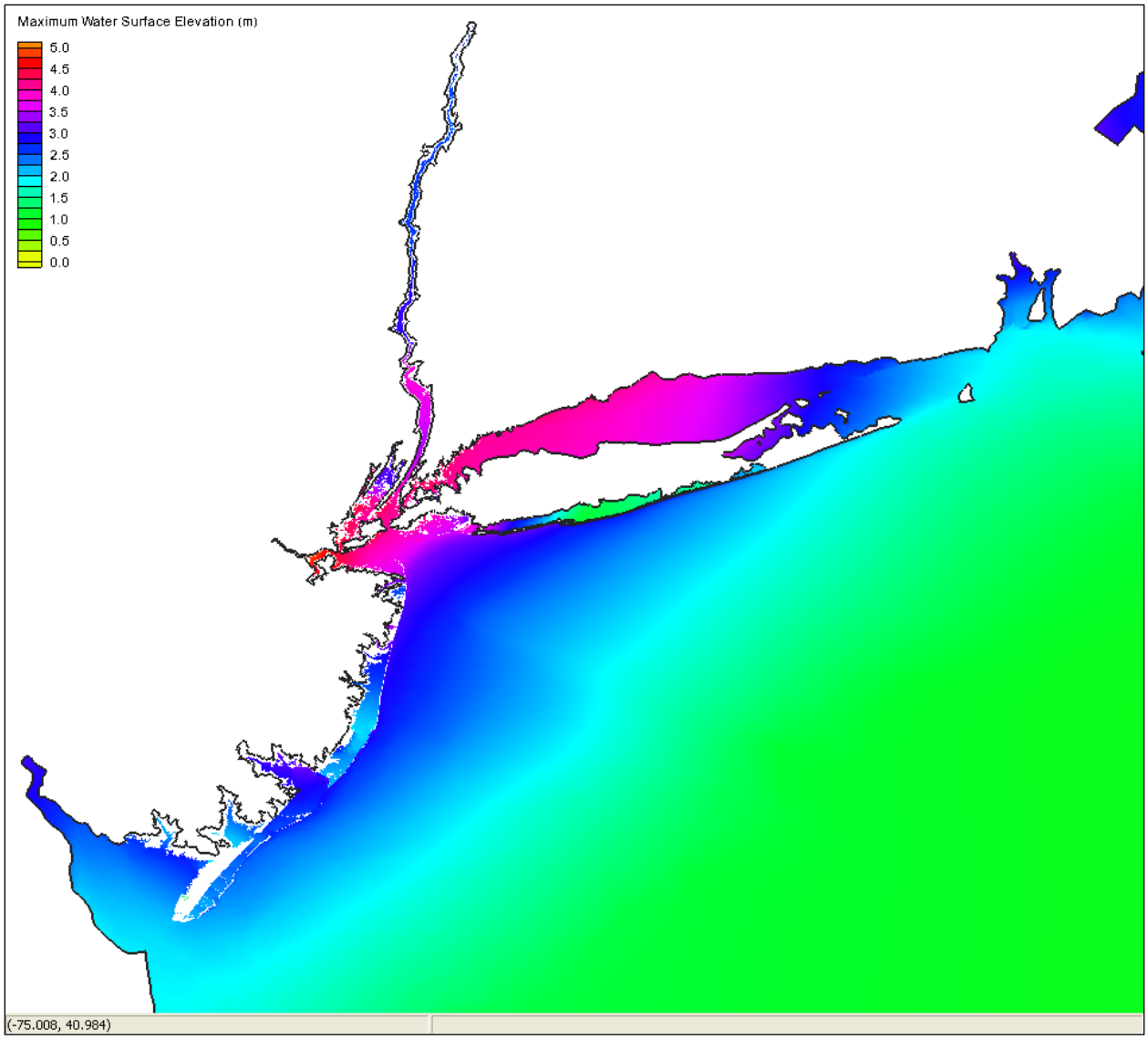

Figure 8. Simulation (measured relative to Mean Sea Level).

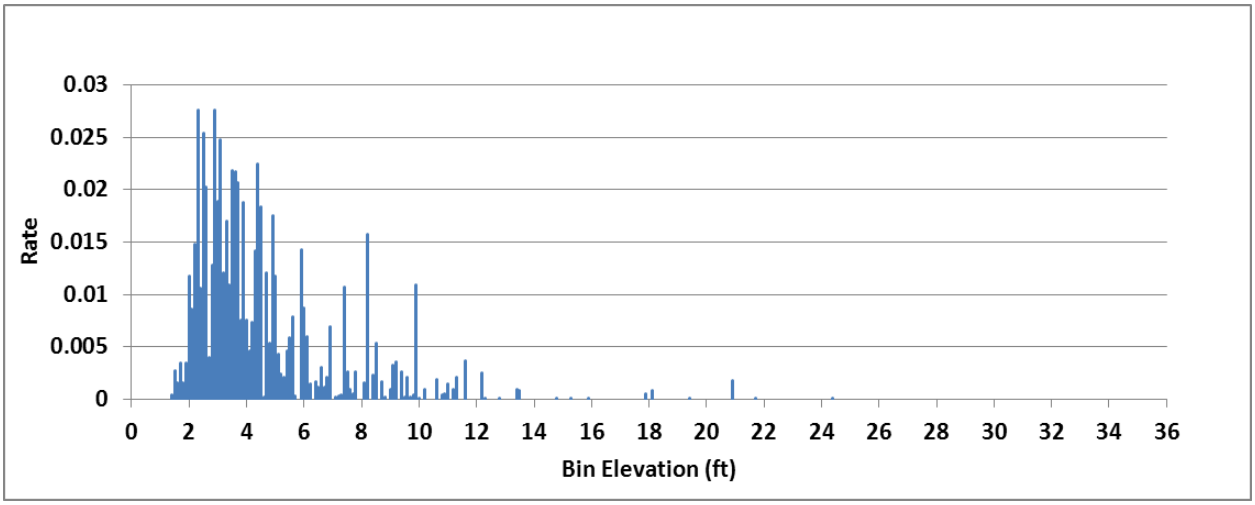

Figure 9. Histogram generated for a single JPM point based on surges and event probabilities

An example of this spreading-out is shown in Figure 10 for the contents of a single bin. The result after redistribution of all the bins is illustrated in Figure 11.

2.3.2 Evaluation of the Epsilon Components

The ε_j term, referred to as the "epsilon term," is designed to include all of the causes for deviations of actual storm surges from the estimates obtained using numerical models of TCs. The ε_j terms applied in this study are described below:

ε_M: Measurement Uncertainty - Standard deviation of measurement uncertainty based on groupings of high water marks (HWMs)

ε_C: Validation Uncertainty - Standard deviation of validation uncertainty: model vs. measured at HWM and Gage Peaks

ε_S: Use of Single vs. Double Exponential Function for Wind Fields - Standard deviation of differences in surges from simulations using single and double exponential wind field. .

ε_I: Use of Idealized Wind Fields rather than Actual Wind Fields - Standard deviation of differences when using idealized and actual wind fields for a simulation.

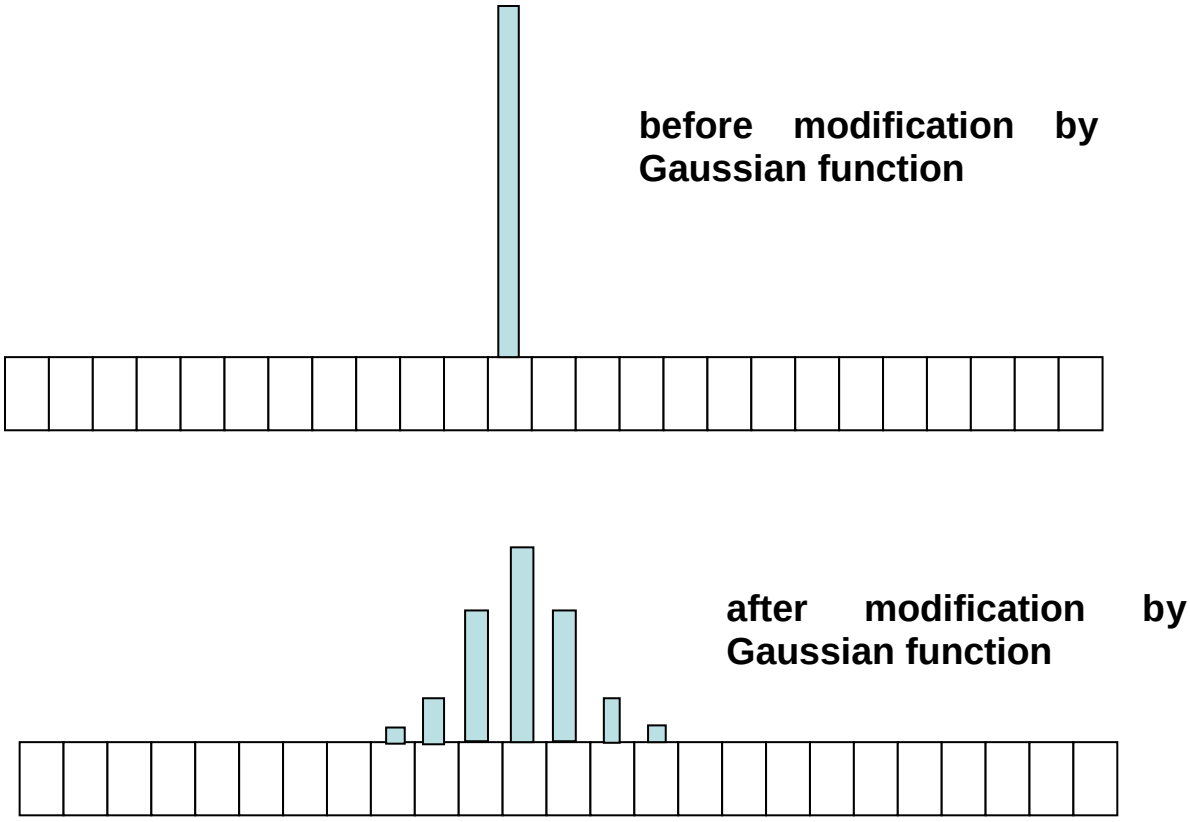

Figure 10. Example application of the Epsilon Terms using the Gaussian Function

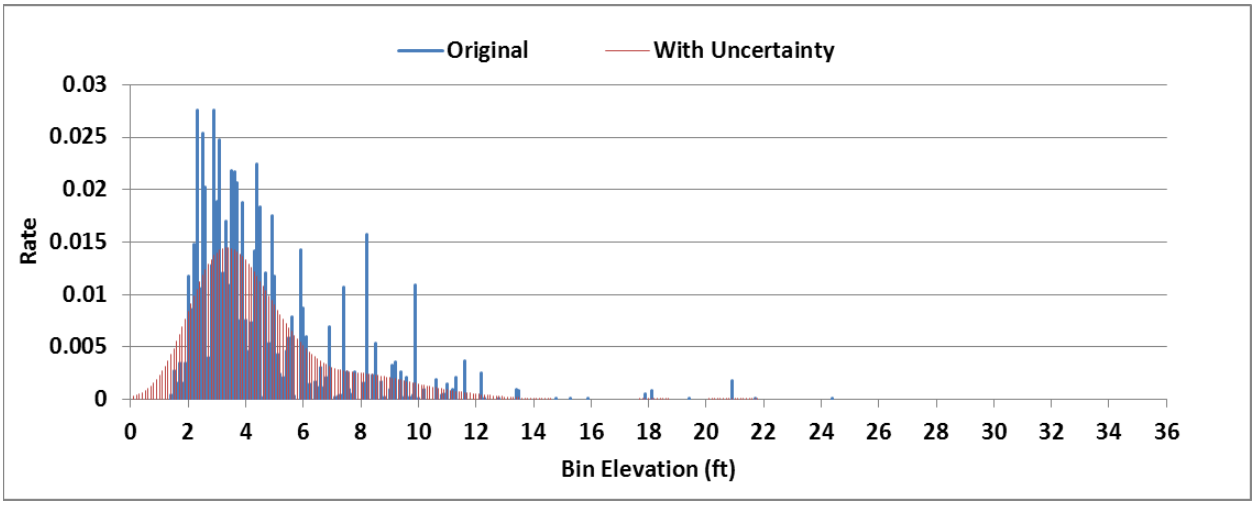

Figure 11. Histogram following the application of the Sigma Term (blue line)

Two other terms often used in the surge studies, the Holland B term and the uncertainty resulting from tide phase, were not applied here because the effects of these terms were directly accounted for in the storm selection process (RAMPP, 2014).

The standard deviation σ_i appearing in Eq. 1 is formed from the individual uncertainty terms according to:

$$\sigma_i = \sqrt{\varepsilon_C^2 - \varepsilon_M^2 + \varepsilon_S^2 + \varepsilon_I^2} \qquad \text{Eq. 3}$$

2.3.2.1 Calculation of Measurement Uncertainty

The measurement uncertainty is estimated by locating clusters of HWM data sufficiently close to yield the same surge elevation. An estimate of the uncertainty is obtained by calculating the difference between each individual measurement in the cluster and the average of the measurements. Twelve suitable clusters of HWMs were determined for three TCs of hurricane strength (1938, 1944 and 1960) yielding 61 estimates of measurement uncertainty. The cluster locations are shown in Figure 12. The data are summarized in Table 2.

Another method for estimating the measurement uncertainty was available for the 1938 storm. Two groups of HWMs were also identified for the 1938 storm, where the surge was expected to increase along the coastline monotonically. A curve was fit to the data to estimate the surge elevation of the group, and the difference between the group's point values and the fitted curve was assumed to be caused by measurement uncertainty. The location of the two groups is shown in Figure 13 and the curve fits are shown in Figure 14. The estimates of the point measurement uncertainty are summarized in Table 3.

The data in the Difference Column in both tables was pooled, and the standard deviation calculated to be 0.54 foot.

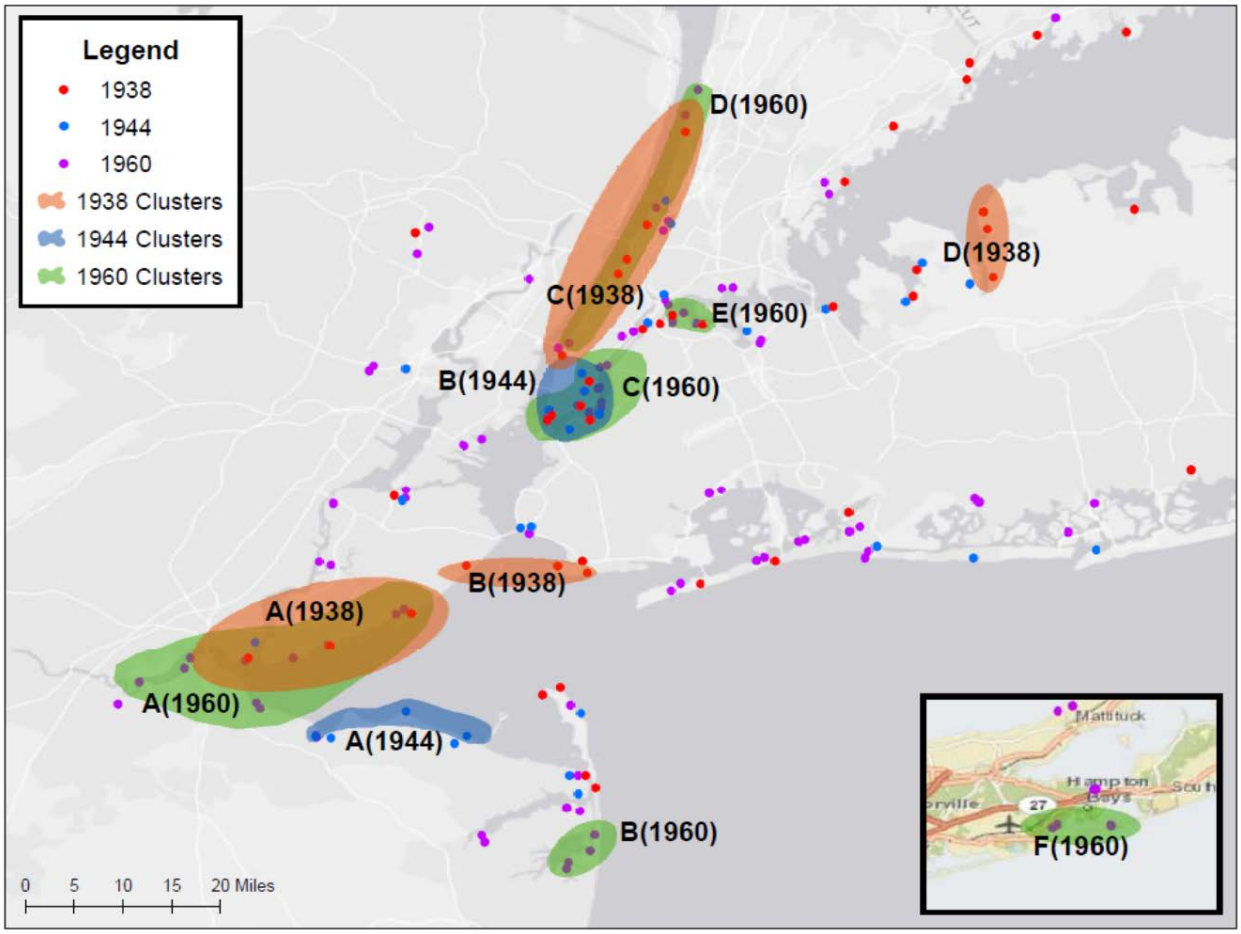

Figure 12. Cluster locations

Figure 13. Group locations

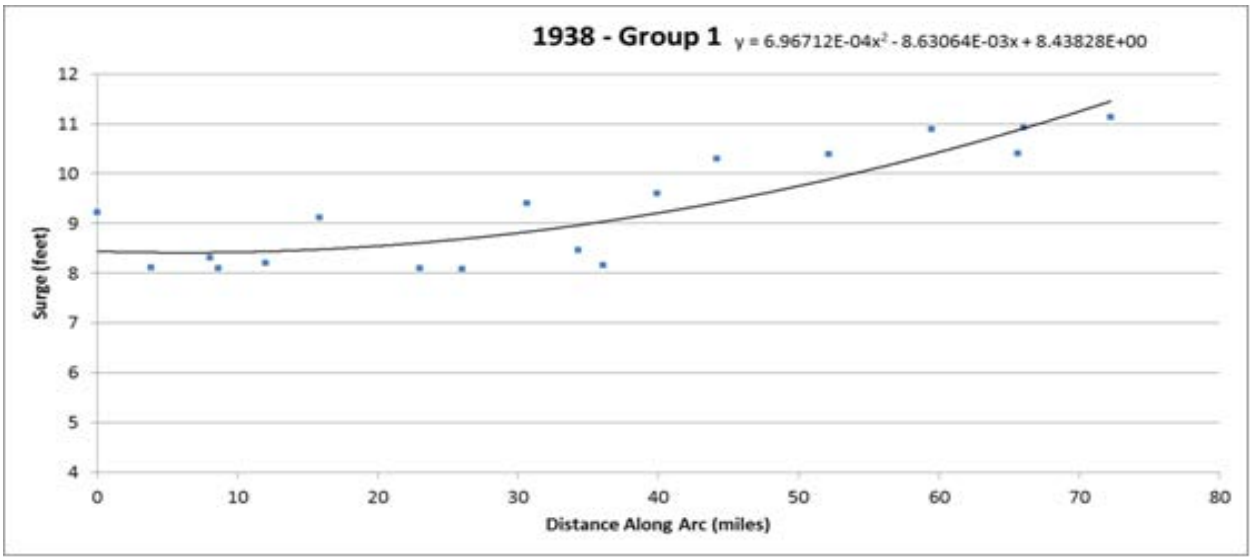

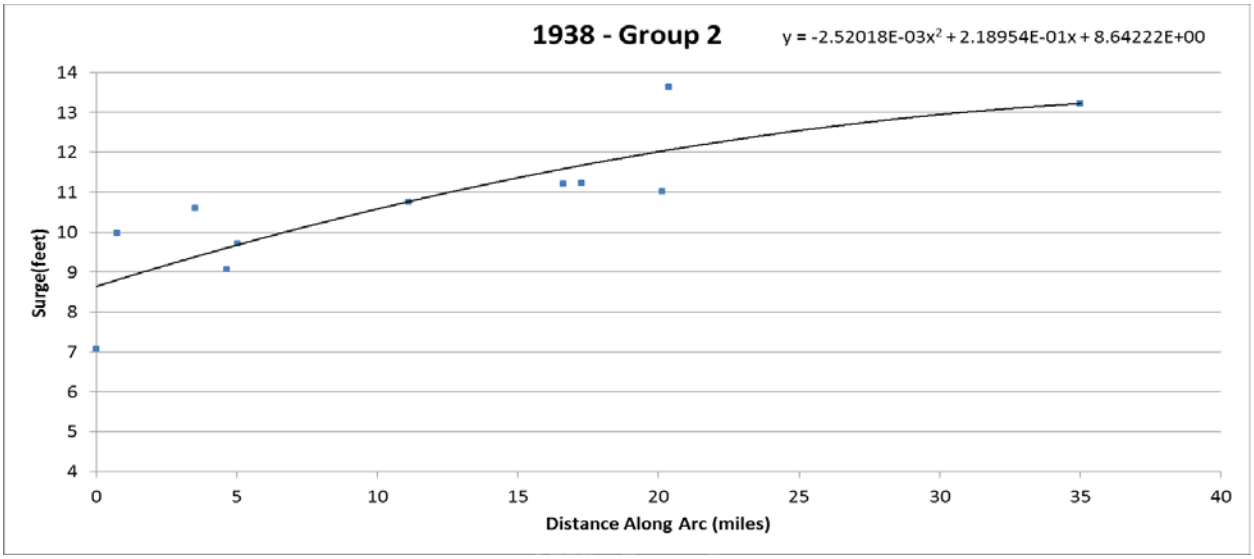

Figure 14. Curve fits

Table 2. Clusters and point estimates of measurement uncertainty

Year	Cluster	Point	Elevation (ft)	Cluster Average (ft)	Difference (ft)
1938	A	1	5.94	6.16	-0.21
1938	A	2	6.22	6.16	0.06
1938	A	3	6.31	6.16	0.15
1938	B	1	6.49	6.92	-0.44
1938	B	2	7.18	6.92	0.26
1938	B	3	7.11	6.92	0.18
1938	C	1	4.73	4.69	0.05
1938	C	2	5.34	4.69	0.65
1938	C	3	3.95	4.69	-0.73
1938	C	4	4.48	4.69	-0.21
1938	C	5	4.93	4.69	0.24
1938	D	1	11.02	11.15	-0.13
1938	D	2	11.22	11.15	0.07
1938	D	3	11.21	11.15	0.06
1944	A	1	8.09	8.04	0.05
1944	A	2	8.03	8.04	-0.01
1944	A	3	7.99	8.04	-0.05
1944	B	1	5.94	5.41	0.53
1944	B	2	5.49	5.41	0.08
1944	B	3	5.29	5.41	-0.11
1944	B	4	4.60	5.41	-0.81
1944	B	5	5.50	5.41	0.10
1944	B	6	5.61	5.41	0.21
1960	A	1	9.50	9.07	0.43
1960	A	2	8.95	9.07	-0.12
1960	A	3	9.09	9.07	0.02
1960	A	4	9.71	9.07	0.64
1960	A	5	9.68	9.07	0.61
1960	A	6	9.33	9.07	0.26
1960	A	7	8.62	9.07	-0.45
1960	A	8	8.94	9.07	-0.12
1960	A	9	8.97	9.07	-0.10
1960	A	10	8.17	9.07	-0.90
1960	A	11	8.79	9.07	-0.28
1960	B	1	5.94	5.79	0.15
1960	B	2	6.24	5.79	0.45
1960	B	3	5.64	5.79	-0.15
1960	B	4	5.34	5.79	-0.45
1960	C	1	7.97	7.15	0.82
1960	C	2	7.18	7.15	0.03
1960	C	3	7.49	7.15	0.34
1960	C	4	7.32	7.15	0.17

Year	Cluster	Point	Elevation (ft)	Cluster Average (ft)	Difference (ft)
1960	C	5	7.36	7.15	0.21
1960	C	6	7.29	7.15	0.14
1960	C	7	6.90	7.15	-0.25
1960	C	8	6.70	7.15	-0.45
1960	C	9	6.60	7.15	-0.55
1960	C	10	6.71	7.15	-0.44
1960	D	1	6.85	6.38	0.47
1960	D	2	6.43	6.38	0.05
1960	D	3	6.00	6.38	-0.39
1960	D	4	6.26	6.38	-0.13
1960	E	1	5.82	6.36	-0.54
1960	E	2	7.11	6.36	0.75
1960	E	3	7.33	6.36	0.97
1960	E	4	5.12	6.36	-1.24
1960	E	5	6.42	6.36	0.06
1960	F	1	4.31	4.22	0.09
1960	F	2	4.72	4.22	0.50
1960	F	3	3.67	4.22	-0.55
1960	F	4	4.19	4.22	-0.03

Table 3. Groups and point estimates of measurement uncertainty

Year	Group	Distance (mi)	Curve Fit Elevation (ft)	Measured Elevation (ft)	Difference (ft)
1938	1	0.00	9.22	8.44	0.78
1938	1	3.87	8.12	8.42	-0.30
1938	1	8.08	8.30	8.41	-0.11
1938	1	8.69	8.09	8.42	-0.33
1938	1	12.11	8.20	8.44	-0.23
1938	1	15.96	9.11	8.48	0.63
1938	1	23.15	8.09	8.61	-0.52
1938	1	26.15	8.08	8.68	-0.61
1938	1	30.84	9.39	8.83	0.57
1938	1	34.51	8.45	8.96	-0.51
1938	1	36.28	8.16	9.03	-0.87
1938	1	40.13	9.60	9.20	0.40
1938	1	44.41	10.29	9.42	0.88
1938	1	52.44	10.39	9.88	0.51
1938	1	59.83	10.89	10.39	0.50
1938	1	66.03	10.39	10.87	-0.48
1938	1	66.41	10.91	10.91	0.01
1938	1	72.68	11.13	11.45	-0.32

Year	Group	Distance (mi)	Curve Fit Elevation (ft)	Measured Elevation (ft)	Difference (ft)
1938	2	0.00	7.07	8.64	-1.57
1938	2	0.74	9.97	8.80	1.17
1938	2	3.56	10.60	9.38	1.22
1938	2	4.68	9.06	9.61	-0.55
1938	2	5.06	9.70	9.68	0.02
1938	2	11.19	10.75	10.77	-0.02
1938	2	16.71	11.21	11.58	-0.37
1938	2	17.38	11.22	11.67	-0.46
1938	2	20.24	11.02	12.03	-1.01
1938	2	20.48	13.63	12.06	1.57
1938	2	35.22	13.21	13.22	-0.01

2.3.2.2 Calculation of Validation Uncertainty

A comparison of the simulated surge and measured surge at the HWM and gage peak values was made for each of the validation storms. There are 216 individual comparisons. A summary of the point estimates of validation uncertainty is shown in Table 4.

The standard deviation of the differences was calculated to be 1.44 feet.

Table 4. Summary of validation uncertainty

Storm	Type	Measured (ft)	Modeled (ft)	Difference (ft)
H1938	HWM	4.75	2.85	-1.90
H1938	HWM	7.06	3.79	-3.27
H1938	HWM	4.22	4.19	-0.03
H1938	HWM	4.37	4.32	-0.05
H1938	HWM	5.61	4.63	-0.98
H1938	HWM	5.00	4.84	-0.16
H1938	HWM	3.48	5.46	1.98
H1938	HWM	5.20	5.58	0.38
H1938	HWM	5.07	5.80	0.73
H1938	HWM	5.66	6.20	0.54
H1938	HWM	6.24	6.22	-0.02
H1938	HWM	10.18	8.14	-2.04
H1938	HWM	10.87	8.91	-1.96
H1938	HWM	11.78	9.42	-2.36
H1938	HWM	9.33	9.57	0.24
H1938	HWM	10.56	10.38	-0.18
H1938	HWM	10.66	10.86	0.20
H1938	HWM	11.16	11.01	-0.15
H1938	HWM	10.66	11.03	0.37
H1938	HWM	10.89	11.19	0.30

Storm	Type	Measured (ft)	Modeled (ft)	Difference (ft)
H1938	HWM	11.48	11.73	0.25
H1938	HWM	11.18	11.84	0.66
H1938	HWM	11.49	11.85	0.36
H1938	HWM	13.18	12.19	-0.99
H1938	HWM	11.40	12.19	0.79
H1938	HWM	13.90	12.61	-1.29
H1938	HWM	13.48	12.67	-0.81
H1938	HWM	12.88	12.69	-0.19
H1938	HWM	0.27	0.00	-0.27
H1938	HWM	3.50	5.14	1.64
H1938	HWM	5.63	6.08	0.45
H1938	HWM	7.51	6.11	-1.40
H1938	HWM	6.70	6.16	-0.54
H1938	HWM	6.62	6.17	-0.45
H1938	HWM	6.89	6.19	-0.70
H1938	HWM	6.71	6.29	-0.42
H1938	HWM	6.34	6.44	0.10
H1938	HWM	7.58	6.49	-1.09
H1938	HWM	5.79	6.52	0.73
H1938	HWM	4.87	6.69	1.82
H1938	HWM	8.18	6.75	-1.43
H1938	HWM	6.24	6.82	0.58
H1938	HWM	6.09	6.29	0.20
H1938	NOAA – Battery, NY	5.90	6.00	0.10
H1938	NOAA - Sandy Hook, NJ	5.00	6.40	1.40
H1944	HWM	6.54	5.18	-1.36
H1944	HWM	5.18	5.55	0.37
H1944	HWM	7.62	5.61	-2.01
H1944	HWM	6.37	6.13	-0.24
H1944	HWM	6.42	6.14	-0.28
H1944	HWM	5.40	6.36	0.96
H1944	HWM	5.62	6.73	1.11
H1944	HWM	5.51	7.15	1.64
H1944	HWM	5.71	7.26	1.55
H1944	HWM	6.16	7.33	1.17
H1944	HWM	6.59	7.33	0.74
H1944	HWM	5.90	7.36	1.46
H1944	HWM	5.83	7.38	1.55
H1944	HWM	4.82	7.40	2.58
H1944	HWM	5.72	7.45	1.73

Storm	Type	Measured (ft)	Modeled (ft)	Difference (ft)
H1944	HWM	6.77	7.45	0.68
H1944	HWM	8.26	7.59	-0.67
H1944	HWM	7.26	7.65	0.39
H1944	HWM	7.69	7.74	0.05
H1944	HWM	5.83	7.75	1.92
H1944	HWM	8.33	8.05	-0.28
H1944	HWM	7.94	8.09	0.15
H1944	HWM	8.31	8.13	-0.18
H1944	HWM	7.63	8.17	0.54
H1944	HWM	8.33	8.22	-0.11
H1944	HWM	8.35	8.25	-0.10
H1944	HWM	7.93	8.29	0.36
H1944	HWM	6.69	8.70	2.01
H1944	HWM	7.43	8.75	1.32
H1944	HWM	7.84	8.99	1.15
H1944	HWM	8.41	9.02	0.61
H1944	NOAA - Atlantic City, NJ	6.90	6.10	-0.80
H1944	NOAA – Battery, NY	5.90	7.30	1.40
H1944	NOAA - Sandy Hook, NJ	7.20	7.70	0.50
H1960	HWM	7.62	7.19	-0.43
H1960	HWM	6.36	3.31	-3.05
H1960	HWM	6.06	3.31	-2.75
H1960	HWM	5.76	3.33	-2.43
H1960	HWM	5.46	3.40	-2.07
H1960	HWM	7.41	4.62	-2.79
H1960	HWM	6.50	4.63	-1.87
H1960	HWM	7.56	5.28	-2.28
H1960	HWM	8.16	5.29	-2.87
H1960	HWM	7.46	5.37	-2.09
H1960	HWM	6.87	5.38	-1.49
H1960	HWM	7.46	6.42	-1.04
H1960	HWM	7.52	6.45	-1.07
H1960	HWM	6.81	6.53	-0.28
H1960	HWM	9.51	6.55	-2.97
H1960	HWM	8.32	6.57	-1.74
H1960	HWM	10.18	6.61	-3.57
H1960	HWM	8.27	6.64	-1.63
H1960	HWM	8.98	6.64	-2.34
H1960	HWM	8.98	6.96	-2.02
H1960	HWM	8.33	7.06	-1.27

Storm	Type	Measured (ft)	Modeled (ft)	Difference (ft)
H1960	HWM	8.29	7.98	-0.31
H1960	HWM	9.26	8.00	-1.26
H1960	HWM	7.60	8.07	0.47
H1960	HWM	8.26	8.27	0.01
H1960	HWM	7.96	8.45	0.49
H1960	HWM	8.63	8.50	-0.13
H1960	HWM	8.69	8.57	-0.12
H1960	HWM	7.57	8.67	1.10
H1960	HWM	8.74	8.72	-0.02
H1960	HWM	9.45	8.80	-0.65
H1960	HWM	6.72	9.22	2.50
H1960	HWM	9.06	9.24	0.17
H1960	HWM	9.07	9.43	0.36
H1960	HWM	9.80	9.44	-0.36
H1960	HWM	8.91	9.47	0.56
H1960	HWM	8.29	9.50	1.21
H1960	HWM	9.21	9.50	0.29
H1960	HWM	8.42	9.63	1.21
H1960	HWM	9.83	9.65	-0.18
H1960	HWM	9.62	9.68	0.06
H1960	HWM	9.09	9.71	0.61
H1960	HWM	10.11	9.81	-0.30
H1960	HWM	9.53	9.83	0.30
H1960	HWM	7.07	4.29	-2.78
H1960	HWM	6.08	4.50	-1.57
H1960	HWM	6.93	4.65	-2.28
H1960	HWM	6.34	5.62	-0.72
H1960	HWM	5.93	6.06	0.13
H1960	HWM	6.77	6.14	-0.63
H1960	HWM	7.58	6.58	-1.00
H1960	HWM	8.39	6.60	-1.79
H1960	HWM	9.39	6.63	-2.76
H1960	HWM	8.67	6.69	-1.98
H1960	HWM	6.51	7.09	0.58
H1960	HWM	8.21	7.16	-1.05
H1960	HWM	7.22	7.16	-0.06
H1960	HWM	6.78	7.17	0.39
H1960	HWM	6.09	7.22	1.12
H1960	HWM	7.26	7.28	0.02
H1960	HWM	6.79	7.29	0.50

Storm	Type	Measured (ft)	Modeled (ft)	Difference (ft)
H1960	HWM	7.40	7.29	-0.11
H1960	HWM	6.78	7.32	0.54
H1960	HWM	6.68	7.33	0.64
H1960	HWM	7.57	7.34	-0.23
H1960	HWM	7.44	7.40	-0.04
H1960	HWM	6.98	7.45	0.47
H1960	HWM	7.58	7.60	0.02
H1960	HWM	7.89	7.79	-0.10
H1960	HWM	8.05	7.86	-0.19
H1960	HWM	7.37	7.99	0.62
H1960	HWM	8.37	8.05	-0.32
H1960	HWM	7.66	8.16	0.50
H1960	HWM	7.41	8.85	1.44
H1960	HWM	6.00	8.86	2.86
H1960	HWM	5.90	9.03	3.13
H1960	HWM	6.50	9.08	2.58
H1960	HWM	7.19	9.08	1.89
H1960	HWM	7.19	9.67	2.48
H1960	HWM	6.62	9.67	3.06
H1960	HWM	6.29	9.68	3.39
H1960	HWM	5.60	9.71	4.10
H1960	HWM	6.09	9.89	3.79
H1960	HWM	6.78	9.89	3.11
H1960	NOAA - Atlantic City, NJ	5.10	4.82	-0.28
H1960	NOAA – Montauk, NY	4.20	6.33	2.13
H1960	NOAA – Battery, NY	7.50	7.82	0.32
H1960	NOAA - Sandy Hook, NJ	7.70	8.36	0.66
N1984	HWM	4.08	4.25	0.17
N1984	HWM	4.91	4.90	-0.01
N1984	HWM	6.50	5.56	-0.94
N1984	HWM	6.02	6.86	0.84
N1984	HWM	7.14	7.85	0.71
N1984	HWM	7.81	9.12	1.31
N1984	NOAA – Montauk, NY	3.61	3.87	0.26
N1984	NOAA - Cape May, NJ	5.12	6.28	1.16
N1984	NOAA - Atlantic City, NJ	5.38	6.87	1.49
N1984	NOAA - Sandy Hook, NJ	5.86	6.90	1.03
N1984	NOAA – Battery, NY	5.74	6.95	1.21
N1984	NOAA - Bergen Point, NY	6.01	7.00	0.99
N1984	NOAA - Bridgeport, CT	6.77	7.87	1.10

Storm	Type	Measured (ft)	Modeled (ft)	Difference (ft)
H1985	HWM	5.57	6.09	0.52
H1985	HWM	7.08	6.58	-0.50
H1985	NOAA – Montauk, NY	2.78	3.62	0.84
H1985	NOAA - Barnegat Inlet, NJ	3.65	4.79	1.14
H1985	NOAA - Bergen Point, NY	5.47	6.60	1.13
H1985	NOAA - Bridgeport, CT	6.75	6.70	-0.05
H1985	NOAA – Battery, NY	5.45	7.48	2.03
H1985	NOAA - Cape May, NJ	5.79	7.55	1.76
H1985	NOAA - Sandy Hook, NJ	5.76	7.59	1.83
H1985	NOAA - Atlantic City, NJ	5.96	8.42	2.46
N1992	HWM	5.54	4.65	-0.89
N1992	HWM	6.23	5.29	-0.94
N1992	HWM	6.05	5.89	-0.16
N1992	HWM	6.86	6.19	-0.67
N1992	HWM	6.39	6.36	-0.03
N1992	HWM	7.61	6.78	-0.83
N1992	HWM	7.04	6.84	-0.20
N1992	HWM	6.76	6.90	0.14
N1992	HWM	7.66	6.93	-0.73
N1992	HWM	7.42	7.32	-0.10
N1992	HWM	7.16	7.73	0.57
N1992	HWM	6.71	7.93	1.22
N1992	HWM	6.99	7.98	0.99
N1992	HWM	7.74	8.42	0.68
N1992	HWM	8.46	9.30	0.84
N1992	HWM	9.21	10.78	1.57
N1992	HWM	10.27	10.78	0.51
N1992	HWM	8.47	11.01	2.54
N1992	HWM	10.21	13.11	2.90
N1992	NOAA – Montauk, NY	4.44	5.27	0.83
N1992	NOAA - Barnegat Inlet, NJ	4.94	5.33	0.39
N1992	NOAA - Cape May, NJ	5.53	6.36	0.83
N1992	NOAA - Atlantic City, NJ	6.37	6.90	0.53
N1992	NOAA – Battery, NY	6.92	8.38	1.46
N1992	NOAA - Sandy Hook, NJ	7.26	8.94	1.68
N1992	NOAA – Bridgeport, CT	8.20	10.06	1.86

2.3.2.3 Calculation of Uncertainty Due to Use of Single vs. Double Exponential Function for Wind Fields

An estimate of the uncertainty that occurs when using a single exponential rather than a double exponential wind field in the surge simulations was developed by comparing the surge values at 16 points for surge results simulated with both a single and a double exponential function. The comparisons were made at the 16 points for five different storms, creating 80 individual comparisons. The storms used for the comparisons and a summary of the surge values at the 16 points for the single and double exponential cases are shown in Table 5.

The data were first analyzed to determine whether the standard deviation of the differences varied with the surge elevation. The average surge elevation was calculated for each comparison and the data were sorted from highest to lowest average surge. Then a "sliding" standard deviation of the surge differences was calculated using a 13-point template (6 points at lower surge and 6 points at a higher surge). A plot of the standard deviation vs. surge elevation was made and is shown in Figure 15. A trend line indicates that the standard deviation of the differences decreases slightly, but the slope of the line is 0.0153. Therefore, the standard deviation was assumed to be constant and calculated as the standard deviation of the differences for the 80 points. The standard deviation value is 0.29 foot.

Table 5. Storms used for the comparisons and a summary of the surge values at the 16 points for the single and double exponential cases.

Observation Station	Surge Single Exp (m)					Surge Double Exp (m)				
	1944 Storm: 1944 Great Atlantic Hurricane	1954 Storm: Hurricane Carol	1955 Storm: Hurricane Diane	1985 Storm: Hurricane Gloria	1999 Storm: Hurricane Floyd	1944 Storm: 1944 Great Atlantic Hurricane	1954 Storm: Hurricane Carol	1955 Storm: Hurricane Diane	1985 Storm: Hurricane Gloria	1999 Storm: Hurricane Floyd
Brandywine Shoal Light/DE Bay	0.918	0.539	0.325	1.768	1	1.079	0.662	0.71	1.66	1.119
Atlantic City, NJ	1.117	0.799	0.197	2.085	0.947	1.246	0.821	0.424	2.102	1.106
Seaside Heights, NJ	1.184	0.995	0.194	1.798	0.744	1.288	1.012	0.331	1.714	0.835
Sandy Hook/Queens Co	1.419	1.259	0.278	2.059	0.772	1.542	1.189	0.416	2.059	0.962
Battery, NY	1.538	1.344	0.294	2.202	0.742	1.594	1.272	0.374	2.227	0.968
Jones Beach, NY	1.972	1.815	0.443	2.716	0.923	1.975	1.735	0.499	2.747	1.106
Fire Island, NY	1.606	1.719	0.259	1.693	0.577	1.567	1.68	0.262	1.718	0.705
Westhampton, NY	1.472	1.794	0.238	1.398	0.506	1.412	1.772	0.235	1.449	0.607
Southampton, NY	1.234	1.722	0.235	1.155	0.433	1.163	1.713	0.235	1.155	0.51
Amagansett, NY	1.484	1.307	0.419	2.123	1.045	1.641	1.245	0.605	2.072	1.242
LIS – Willets Pt	1.864	2.315	0.476	1.591	0.978	1.911	2.258	0.432	1.698	1.019
LIS – Westchester Co	1.718	2.16	0.428	1.407	0.934	1.773	2.105	0.438	1.329	0.964
LIS – Stamford	1.585	1.891	0.355	1.292	0.868	1.67	1.85	0.382	1.186	0.948
LIS – Bridgeport	1.59	1.877	0.315	1.139	0.794	1.708	1.853	0.328	1.153	0.944
LIS – New Haven	1.709	2.015	0.272	1.648	0.847	1.823	2.006	0.286	1.619	0.971
LIS – Gardiners Island	1.618	1.885	0.268	1.436	0.696	1.674	1.893	0.262	1.427	0.773

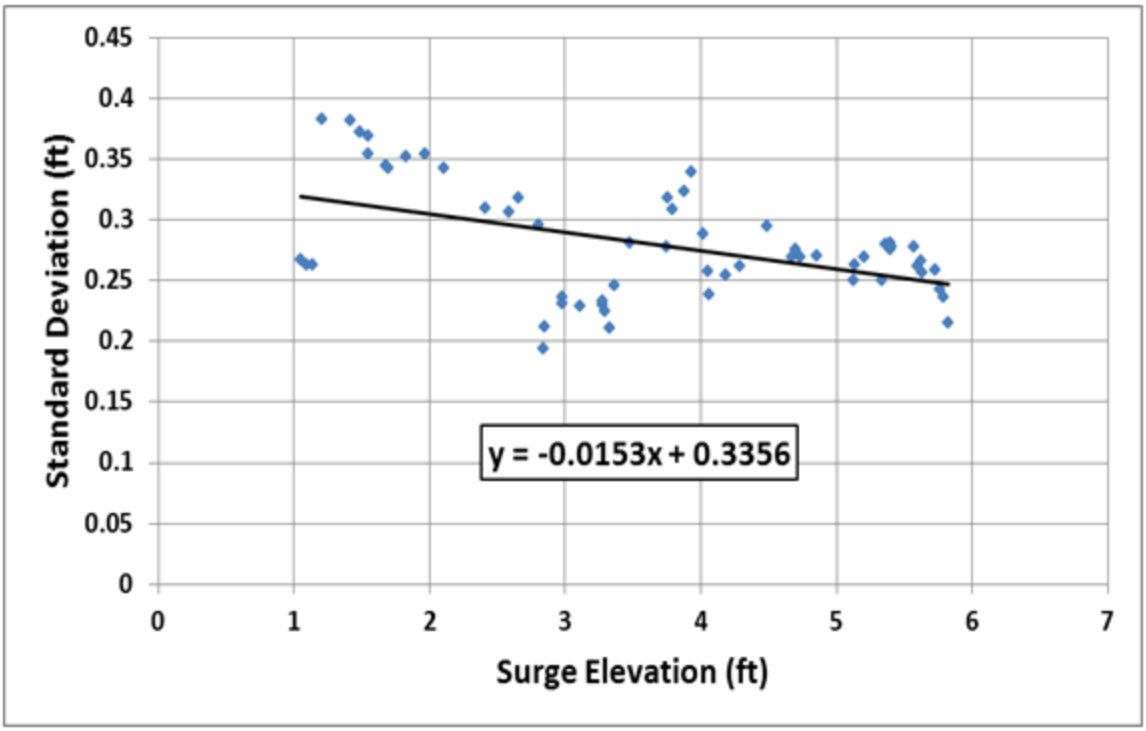

Figure 15. Standard Deviation vs. Surge Elevation

2.3.2.4 Use of Idealized Wind Fields Rather than Actual Wind Fields

The uncertainty for the use of the idealized winds rather than the actual winds was estimated by Dr. Vince Cardone of Oceanweather Inc. to be approximately 1.5 times the value used in the Mississippi Study (URS, 2008), which was 1.17 feet. The value for the uncertainty term is therefore 1.76 feet.

2.3.2.5 Summary of Final Values

Values (in feet):

ε_M: 0.54

ε_C: 1.44

ε_S: 0.29

ε_I: 1.76

The epsilon values were combined according to Eq. 3 for input into the SURGE_STAT model. The final value of the uncertainty term σ_i is 2.2 feet.

2.4 COMBINING RESULTS FOR THE EXTRATROPICAL AND TROPICAL CYCLONES

To complete the analysis, the total stillwater return interval analysis involves combining the frequencies associated with even increments of the surge elevations from both TCs and extratropical storms. For each elevation bin there is an annual recurrence frequency associated with both storm types. The total frequency is simply the sum of these. This was computed for all the ADCIRC nodes across the project area.

The modified histogram was then summed from the highest bin to the lowest, resulting in an estimate of the cumulative surge distribution. This is illustrated in Figure 16, which shows the cumulative probability curve corresponding to the summation of the GEV fit for the extratropical storms and the non-parametric distribution developed for TCs. The surge height for any return interval can then be interpolated from this curve. For example, the stillwater elevation for the 1-percent-annual-chance recurrence interval (0.01 on the vertical axis) for the example JPM point curve in Figure 16 is estimated to be about 14.8 feet. The flood elevations for the 10-, 2-, and 0.2-percent-annual-chance can be similarly obtained by finding the stillwater elevation associated with the 0.1-, 0.02-, and 0.002-values on the vertical axis.

2.5 QUALITY ASSURANCE

The final stillwater elevations for each annual recurrence interval were checked using two procedures:

1. The surge surfaces were plotted in SMS (Zundel, 2000) using color contours and were viewed for anomalies.
2. The surge values for each JPM point for each recurrence interval were checked for consistency. For instance, the elevation for the 0.2-percent-annual-chance recurrence interval was checked to ensure that it was equal to or greater than the value of the 1-percent-annual-chance recurrence interval.

The final stillwater values were prepared for eventual delivery to FEMA for review, and for review and use by its contractors in subsequent overland wave modeling and mapping tasks.

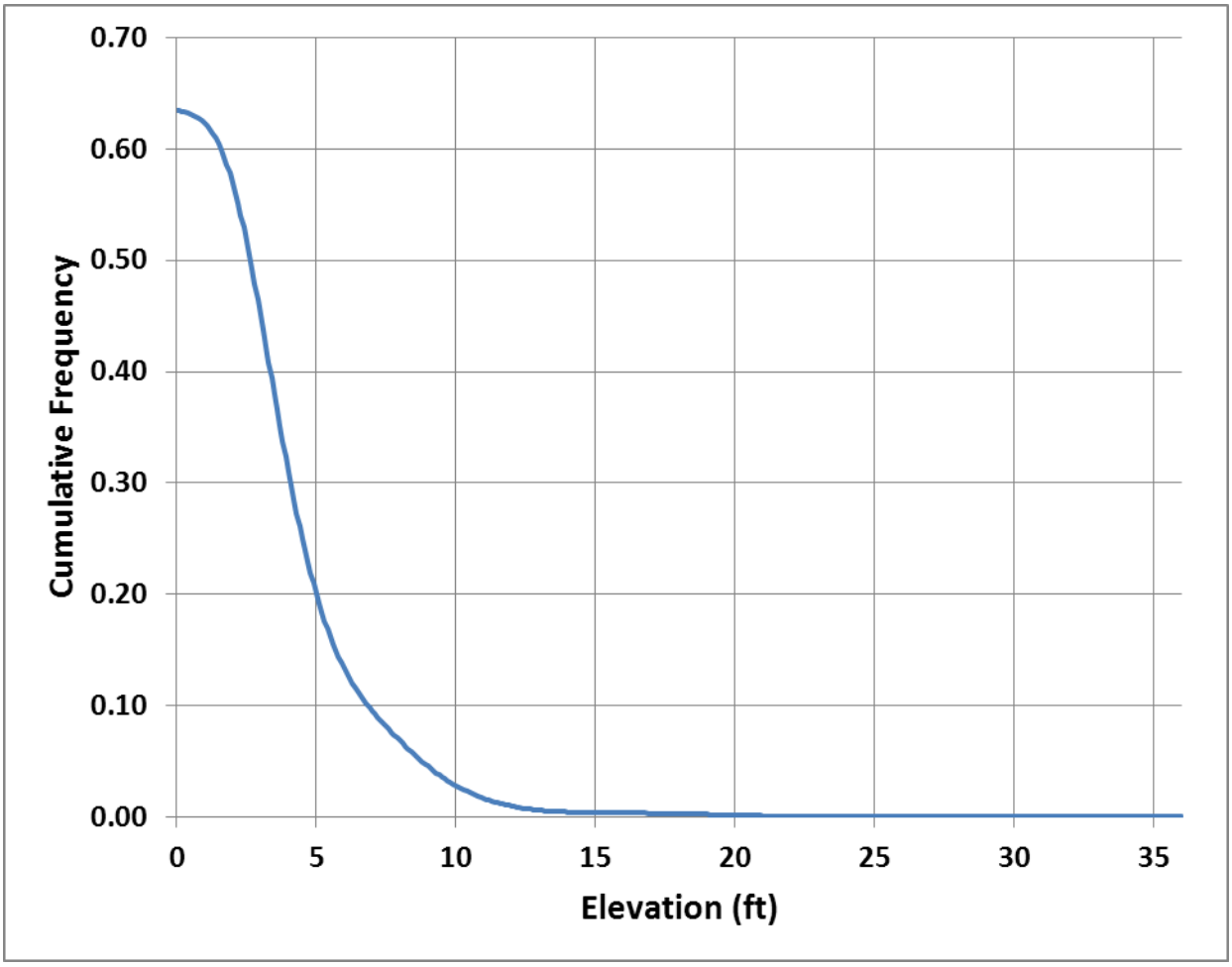

Figure 16. Cumulative probability curve for determination of the return interval stillwater elevations

SECTION THREE STARTING WAVE CONDITIONS

The overland wave modeling requires wave conditions at the starting location of each transect. . The approach for developing the starting wave conditions in this study was based on the same approach used in the Mississippi Coastal Flood Study (URS, 2008), the Franklin Wakulla Jefferson Study (Slinn, 2010), the Florida Panhandle and Alabama Study (Slinn, 2013), and the North Carolina Study (Blanton, 2012). Additionally, the basic procedure was described to contractors conducting similar studies in FEMA Region III, and has subsequently been adopted for Region III studies.

A wave processing methodology was developed to determine the wave conditions associated with the 1-percent-annual-chance exceedance level. The processing was applied to a swath of ADCIRC-UnSWAN (ADCIRC coupled with Unstructured version of SWAN, or the Simulating WAves Nearshore model) output points (nodes) in the vicinity of the coastline throughout the entire study area and stored in a database. The swath was defined by drawing a polygon that included the land portion of the model mesh, and extending it offshore of the coastline approximately 1 to 3 kilometers (km). A filter was then applied to eliminate nodes with water depths less than 0.5 feet, which ensured that the final selected nodes were located offshore. This database contained data for approximately 147,000 offshore nodes and was eventually filtered down to approximately 138,000 nodes through the Quality Assurance/Quality Control (QA/QC) process.

At each ADCIRC-UnSWAN model node in the swath, all production run results were identified and gathered for analysis. The process for determining the starting wave conditions was then applied independently for each ADCIRC-UnSWAN node.

The data collected for each node was organized by storm and includes columns for the storm ID, the maximum surge elevation, the significant wave height, and the peak wave period. The results for the simulated TCs and extratropical storms were pooled together for the wave analysis. The wave height and period are those that occurred at the time of the maximum surge elevation. An example of the data format is shown in Figure 17. The data were sorted by surge elevation, from smallest to largest, and plotted. An example of a plot for one node (corresponding to the data shown in Figure 17) is shown in Figure 18. The surge increases monotonically because the data were sorted by the surge elevation. The wave height and period also increase with surge elevation, but some scatter exists in those curves. This scatter occurs because the wave conditions do not correlate perfectly with the surge elevation, and may vary due to differences in wind direction and other factors when the maximum surge elevation occurs.

The starting wave height and period were then selected to correspond to the 1-percent-annual-chance exceedance level. For the node represented in Figure 18, the 1-percent-annual-chance exceedance level is designated by the square symbol, and is 1.8 m. The associated wave height and period are designated in the figure by the cross symbols and are 0.84 m and 2.15 seconds (s), respectively. In order to account for the scatter in wave height and period data, the average height and period over the seven storms closest to the 1-percent-annual-chance exceedance level were used to obtain the final values.

The QA/QC process consisted of producing a plot similar to that shown in Figure 18 for a randomly selected set of nodes in each county, and visually inspecting it to ensure the data were free from inconsistent and irregular results. Approximately 50 to 150 nodes were selected for each county, depending on the length of the county coastline. Also, for each node that was

processed, the standard deviation of the wave heights and periods used in the averaging process was calculated based on the values extracted from the seven storms surrounding the 1-percent-annual-chance exceedance level. The ratio of the standard deviation to the average value was calculated for both the wave height and the wave period, and these were reviewed to ensure no unusually high values occurred. A filter was then developed to screen for potential outliers. For the wave height, the results were flagged if the ratio exceeded 0.5. For the wave period, which tended to have inherently more scatter, the flagging criterion was set at 1.0.

	B	C	D
1	Surge	Wave Height (m)	Wave Period (s)
2	0.46	0.63	1.58
3	0.48	0.08	1.50
4	0.51	0.08	1.66
5	0.51	0.66	1.67
6	0.52	0.63	1.58
7	0.53	0.64	1.61
8	0.53	0.79	1.70
9	0.54	0.61	1.63
10	0.54	0.62	1.59
11	0.55	0.39	1.64
12	0.57	0.67	1.55
13	0.58	0.68	1.77
14	0.64	0.43	1.52
15	0.67	0.62	1.71
16	0.67	0.59	1.68
17	0.68	0.62	1.69
18	0.68	0.48	1.61
19	0.73	0.46	1.82
20	0.73	0.37	1.70
21	0.74	0.71	1.68
22	0.75	0.65	1.68
23	0.76	0.65	1.79
24	0.76	0.55	1.83
25	0.76	0.73	1.78
26	0.76	0.58	1.75
27	0.76	0.60	1.78

Figure 17. Example data file used for developing wave characteristics

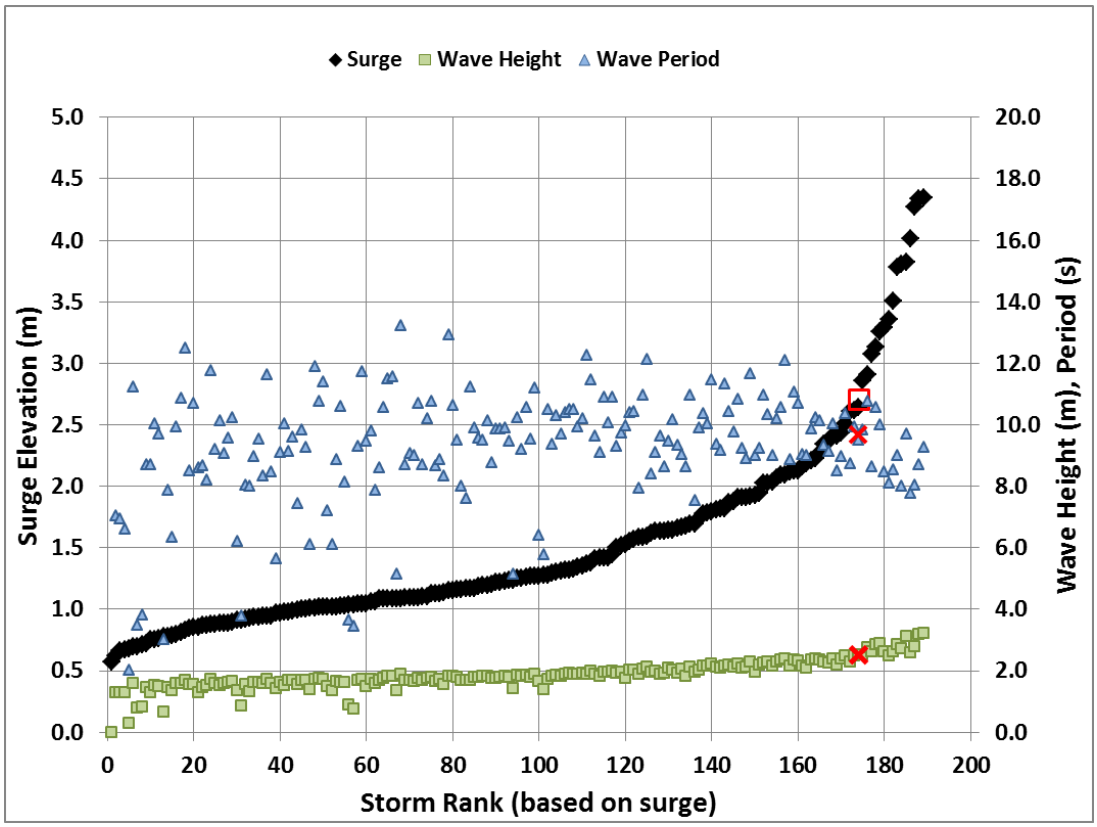

Figure 18. Example of surge and wave data processing to determine the starting wave characteristics

The final wave heights and periods were tabulated for all node locations and made available to the study team for subsequent overland analysis. During the wave data processing, it became apparent that the peak wave period data that were obtained from the production run outputs contained anomalous results that required special attention. The wave heights for each storm were generally more consistent, but occasionally anomalous values would occur. Examples of the peak wave period behavior are shown in Figures 19 through 21, each representing a single storm simulation output. The plots show the distribution of the peak period, the mean period, and the wave height that occurred at the peak surge. The results shown in the plots focus on New York Harbor and Jamaica Bay, but these plot characteristics are representative of conditions along the entire coastline of the study area. The most prolific characteristic of the peak data (Panel a) are the regions, referred to as clusters, where the peak periods are 32 seconds. Some of these clusters of anomalous peak period values appear to occur in all simulations, and some clusters only occur in one or a few simulations. Additionally, for the clusters that appear repeatedly, the extent of the affected area may vary from storm to storm. In all cases, it appears that for the peak period, the affected areas are defined by an abrupt change from expected wave period values to periods of 32 seconds. Subsequent to the completion of the production simulations and the post-processing documented here, wave period issues were identified by ADCIRC-UnSWAN code authors and resolved (Dietrich, 2012). However, the remedies were not available at the time of this study.

The characteristics of the mean period (Panel b) are quite different than those of the peak period. In many of the regions where the peak period anomalies occur, there is no obvious impact on the mean period. In some regions, there is an apparent impact, but the impact is limited to fewer nodes. For example, in one part of Jamaica Bay, the area with anomalous peak period values encompasses 1,200 nodes, but there are only 37 nodes in which the mean period appears to be anomalous. Furthermore, in the area of the impacted mean periods, there is a transition rather than an abrupt change. For instance, for the 37 nodes in which the mean period appears to be anomalous, the mean period at the center of the cluster was 12 seconds. The mean periods at four to six nodes away from this center appear unaffected (approximately 4 -second mean periods), and there is a smooth transition (from 12 to 4 seconds) in the mean period values across the cluster.

A review of the wave height (Panel c) indicated that the impact of the peak period anomalies do not have a profound effect on the wave height. The characteristics of the wave height for Jamaica Bay are shown in more detail in Figure 22. There appears to be some variation in wave height in the bay on the order of 0.5 to 1.2 meters, which is expected. The bathymetry is shown in Panel c, and many of the variations in the wave height correlate with the presence of channels in the bay. However, the wave heights in the areas with significant anomalies in the mean period are systematically higher, on the order of 1.6 meters, than those in the unaffected parts of the bay. This characteristic is demonstrated again in Figure 23, which shows a similar pattern in the vicinity of the entrance to Jamaica Bay. The apparent impacts to the wave height appear to be limited to the regions in which the mean period is impacted.

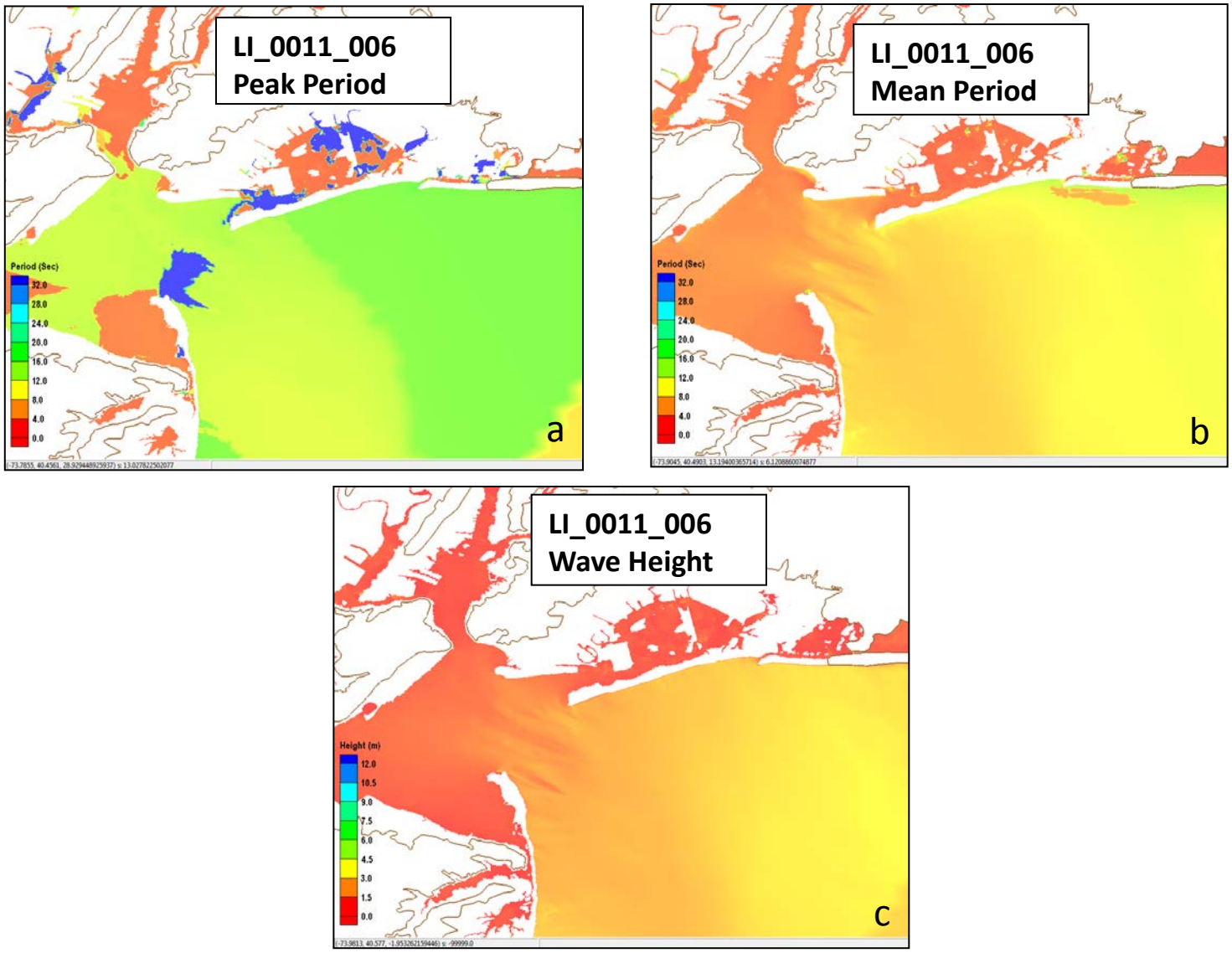

Figure 19. Examples of peak period, mean period, and wave height distribution for a single storm (LI_0011_006)

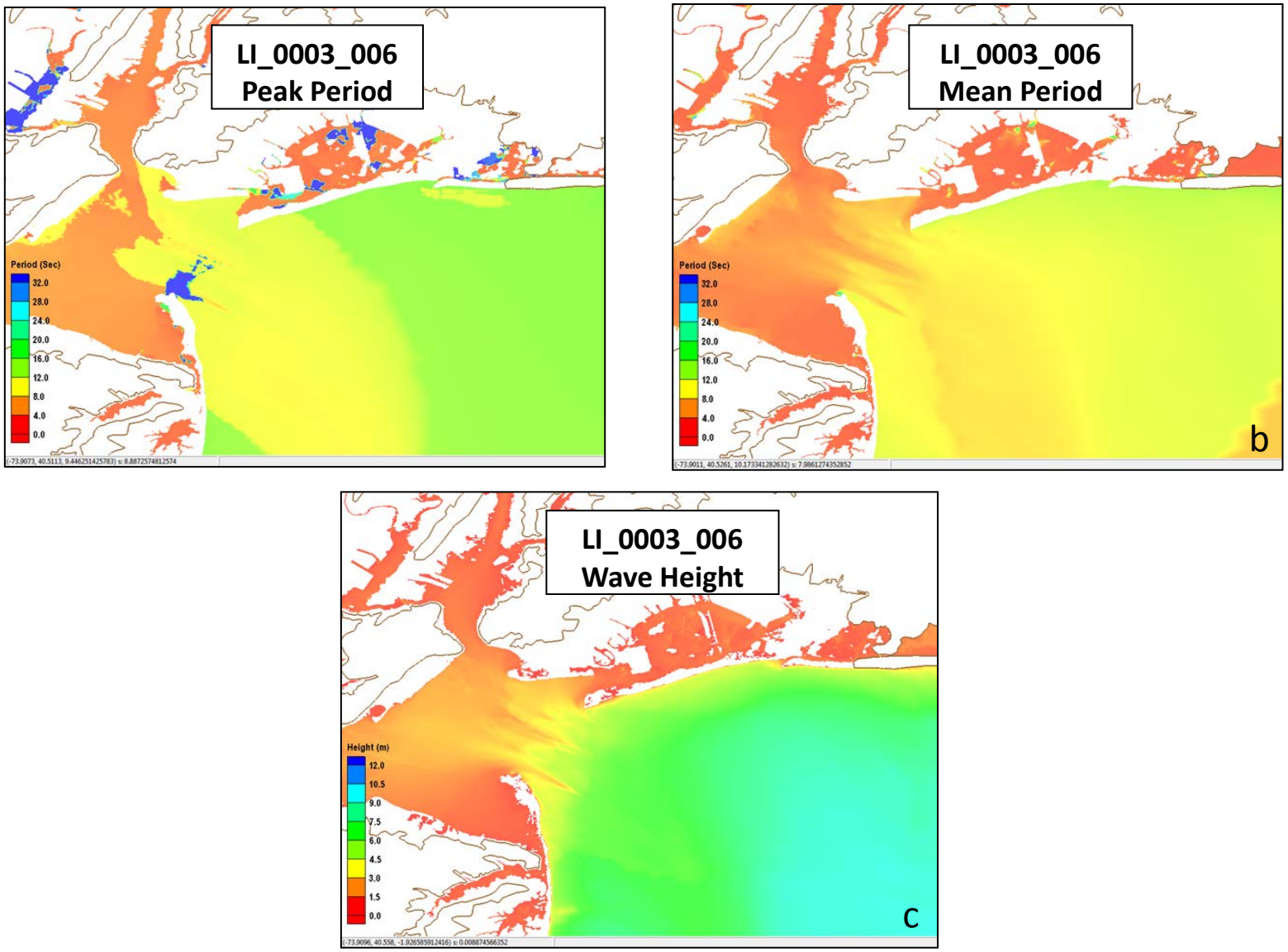

Figure 20. Examples of peak period, mean period, and wave height distribution for a single storm (LI_0003_006)

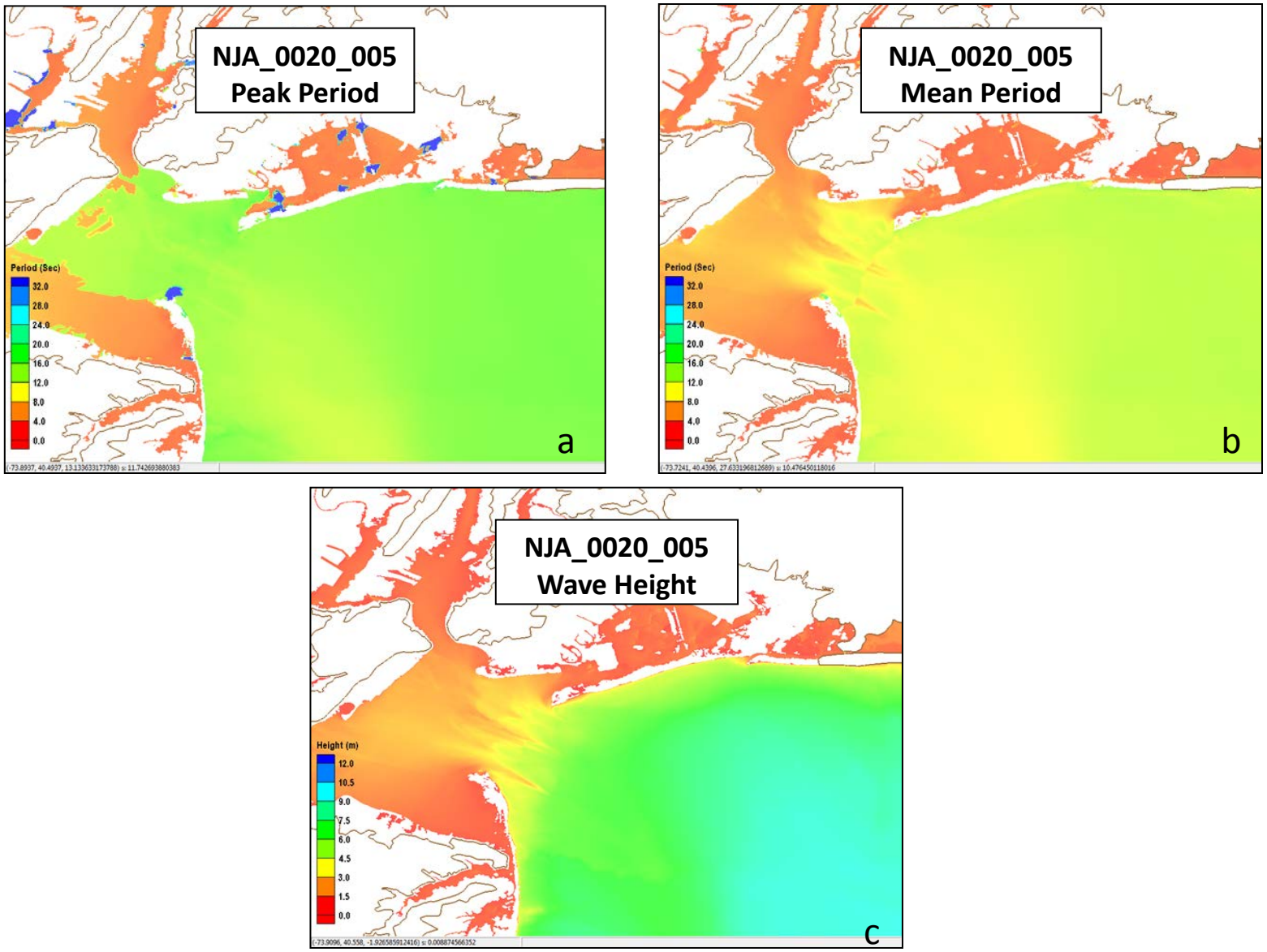

Figure 21. Examples of peak period, mean period, and wave height distribution for a single storm (NJA_0020_005)

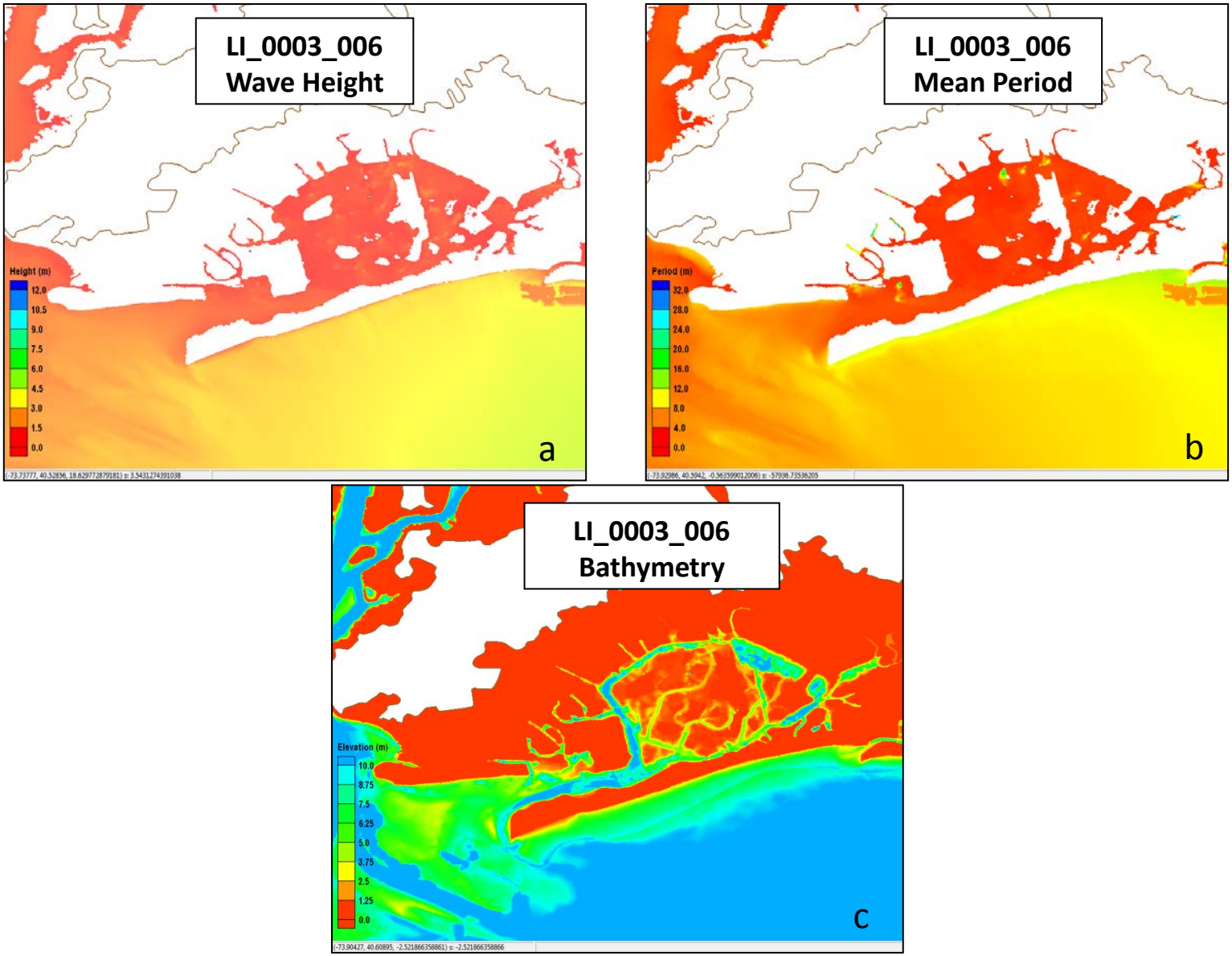

Figure 22. View of wave height, mean period for storm LI_0003_006 and the area bathymetry

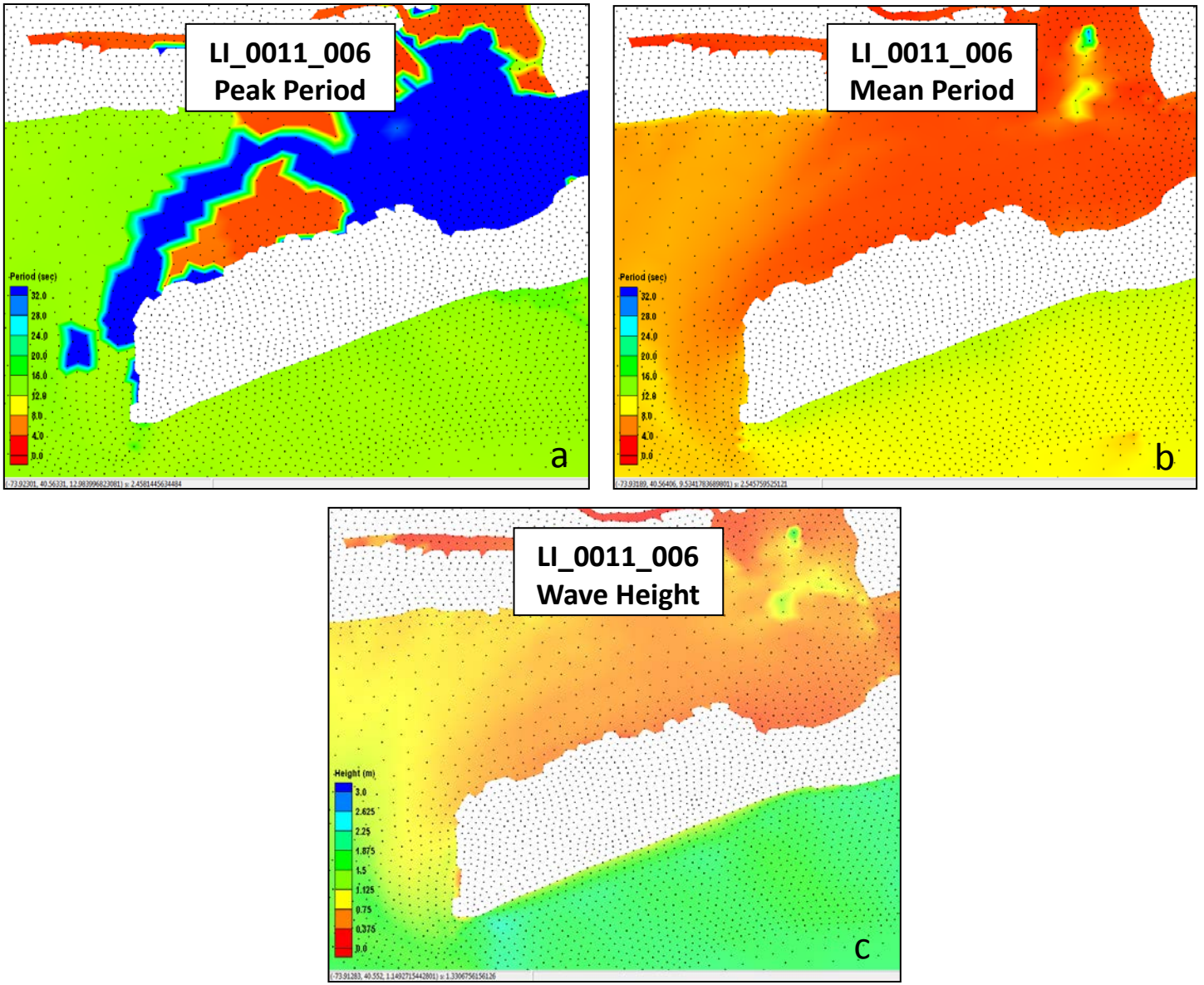

Figure 23. Examples of peak period, mean period, and wave height distribution for storm LI_0011_006 near Jamaica Bay

In summary:

- The anomalies originally detected in the peak period data from the storm simulations appear to occur in discrete clusters with well-defined boundaries.
- Some of the clusters appear in most simulations and others are much less prevalent.
- The impact to the mean period occurs in the same vicinity as some of the anomalous peak period clusters, but is limited to a much smaller area.
- The impacted mean period areas tend to transition to the unaffected values over a few nodes, while the peak period anomalies are characterized by abrupt changes between adjacent nodes.
- The impact to the wave height is limited to the same areas where the mean period is impacted.

An approach for identifying and eliminating nodes with anomalous wave period (and potential wave height) anomalies was developed. The approach ensures that no anomalous results were used as starting conditions for the Wave Height Analysis for Flood Insurance Studies (WHAFIS) analysis, and therefore would also not impact the final Base Flood Elevations.

The WHAFIS model is expecting the peak period as input and the runup methods expect various forms of wave period. However, the relatively large clusters of anomalous peak periods occurring throughout the model prevented a straightforward processing of the wave data. This study is one of the first to use the directly coupled ADCIRC-UnSWAN model for the storm simulations, and the unknown issues with the peak wave period and the subsequent uncertainty in the reliability of the peak period data found in the study results dictated development of an alternate approach for developing the starting peak wave period data. One approach would be to remove the areas with the anomalous peak periods because they are relatively easy to identify. However, removing this data would have left large gaps in the spatial representation of the peak periods, and would reduce confidence in interpolating peak period data across the gaps from nodes on the perimeter.

An alternate approach, which was adopted here, consists of processing the mean wave period results from the storm simulations instead of the peak wave period data. A review of the mean wave period data indicated that the affected areas were significantly smaller in extent, and consequently, the spatial extent of the gaps would be small. Therefore, interpolation of data across the gaps could be completed with confidence.

Two other characteristics of the mean period and wave height data were factored into the final approach. First, the anomalous mean peak data were much more difficult to identify than the peak period anomalies, mainly because the anomalies appeared to transition from good values to anomalous values over a few mesh nodes. Also, unlike the peak period anomalies that always had values of 32 s, the mean period anomalies were not always the same value. Secondly, the impacts to the mean period and wave height appeared to occur inconsistently and were unlikely to have impacted every storm simulation. Because the processing of the wave data focuses only on the seven storms with maximum water elevations in the range of the 1-percent-annual-chance exceedance level, there is a reasonable chance that anomalies that may have occurred only in a few storms would not affect the final wave height and period values for use in the WHAFIS and

runup calculations. Thus, the final approach was to process all of the nodes in the swath and then use post-processing to filter out any nodes with suspect wave characteristics.

The QA/QC process described previously was used to identify when one or more storms with anomalous data were used in the processing. The standard deviation would be much larger for nodes in which anomalous data were used, and these nodes would then be flagged by the QA/QC process. There were a few nodes at which every storm used to calculate the wave characteristics had anomalous data, or if only few storms had anomalies, they were sufficiently large to affect the final wave characteristics. These nodes could be identified by reviewing the spatial pattern of the mean period or wave height data. Figures 24 through 26 show examples of the spatial distribution of the mean period and wave height and how the anomalies appear. Figure 24 shows a region in southern New Jersey. Overall, the wave heights appear to vary smoothly throughout the area; however, there are a few nodes in which the wave heights are significantly larger than the surrounding values. This behavior is attributed to mean period and wave height anomalies.

A similar situation for an area in Jamaica Bay is shown in Figures 25 and 26. The impact is less severe in the Jamaica Bay example because the anomalies appear to be smaller, but the affected areas are visible as a localized area in which the wave period and height increase above the surrounding area. A spatial review was combined with the location of the WHAFIS transect starting locations to identify anomalous results. The review did not identify any issues with the wave conditions in the vicinity of the WHAFIS transect starting locations, and therefore no WHAFIS starting wave condition included anomalous results.

To determine the peak wave periods for overland model input, a scale factor can be selected by reviewing the mean and peak period outputs in areas where they are both free of anomalies, or this factor can be based on theoretical considerations. The scale factor has not been applied to the data developed in this phase of the work, but will be applied prior to the WHAFIS analysis and documented in the subsequent reports for each individual project.

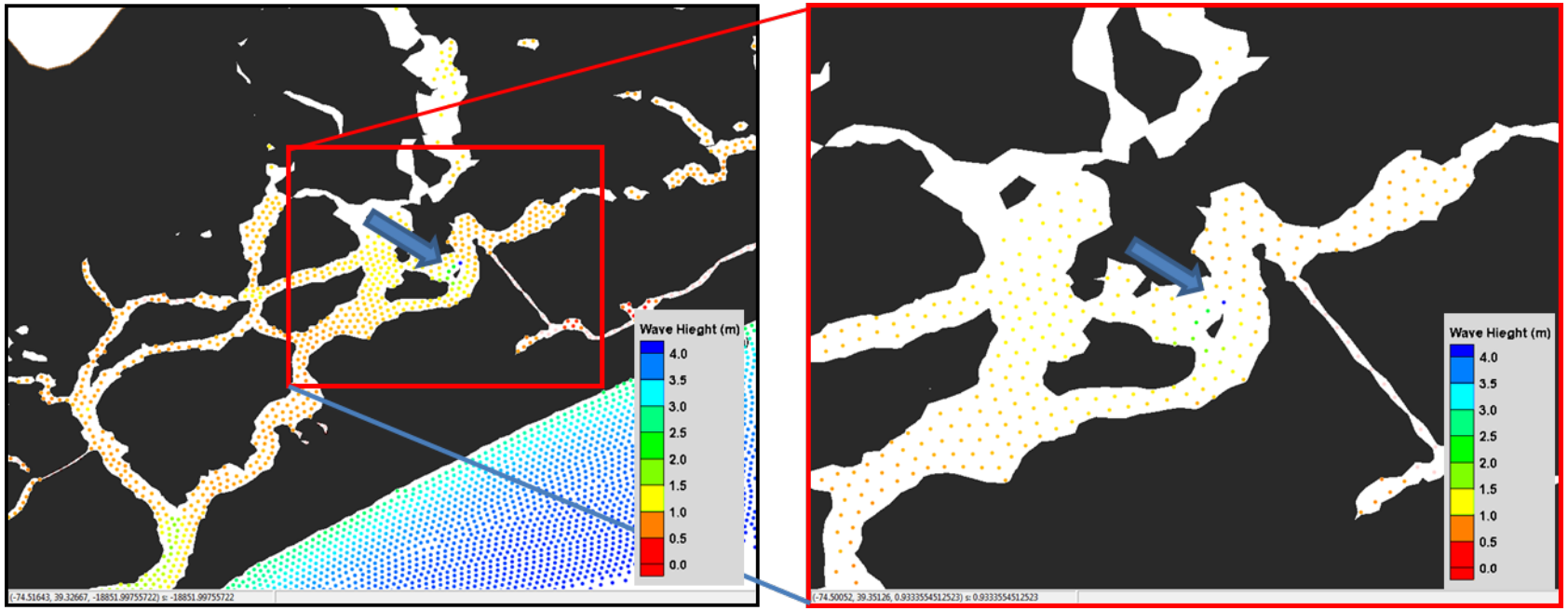

Figure 24. View of starting wave heights at nodes in the southern New Jersey area

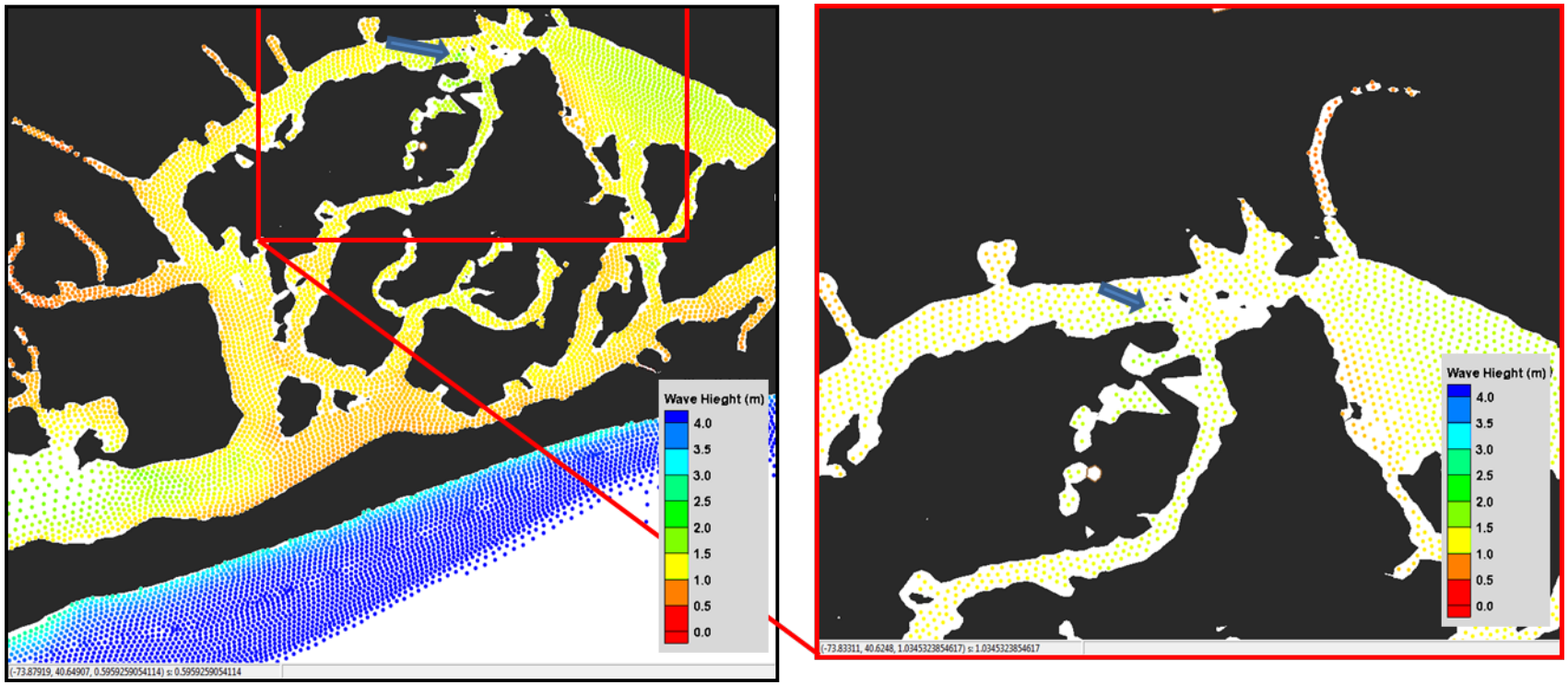

Figure 25. View of starting wave heights at nodes in the vicinity of Jamaica Bay

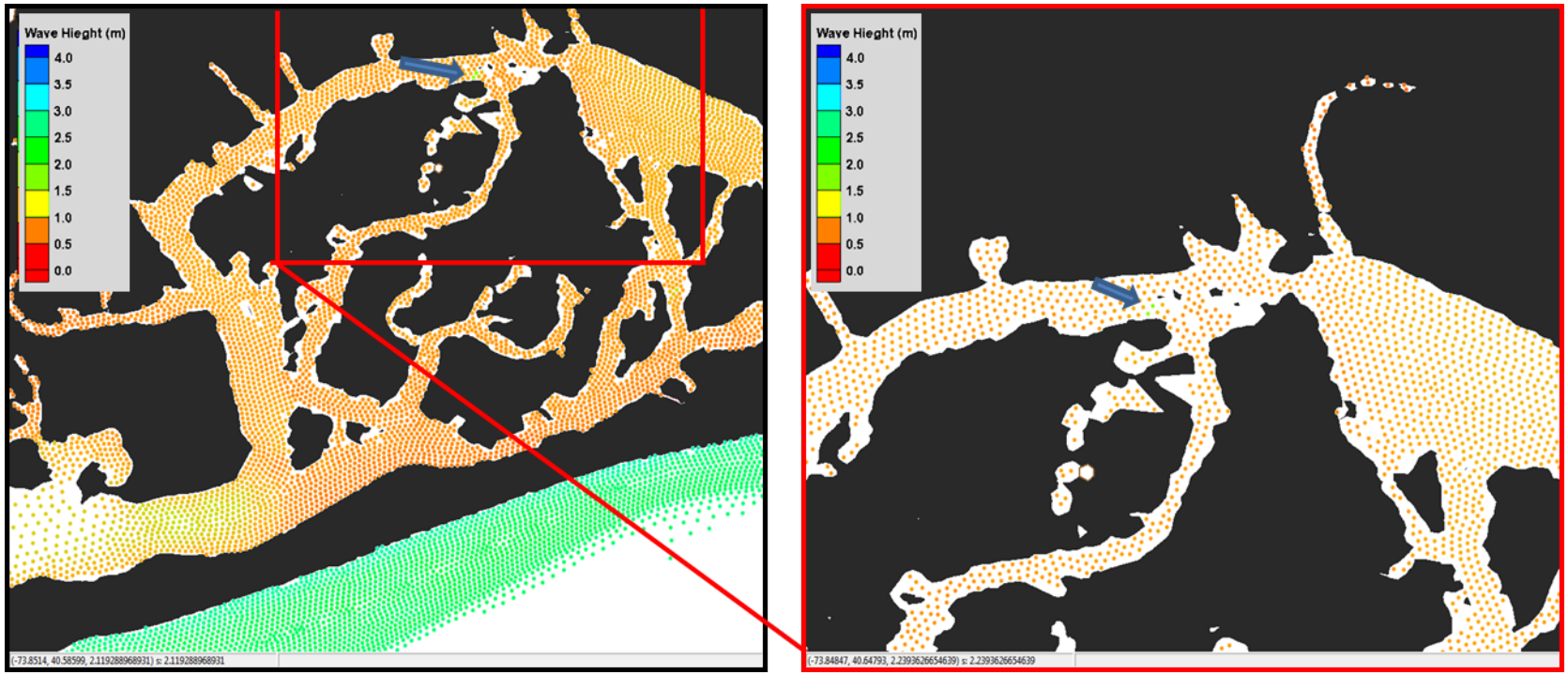

Figure 26. View of starting wave periods at nodes in the vicinity of Jamaica Bay

SECTION FOUR REFERENCES

Blanton, Brian, et al. September 5, 2012. North Carolina Floodplain Mapping Program, Report on Production Simulations and Statistical Analysis.

JC Dietrich, M Zijlema, P-E Allier, LH Holthuijsen, N Booij, JD Meixner, JK Proft, CN Dawson, CJ Bender, A Naimaster, JM Smith, JJ Westerink. 2012. "Limiters for Spectral Propagation Velocities in SWAN." Ocean Modelling, in press, DOI: 10.1016/j.ocemod.2012.11.005.

Fugro William Lettis and Associates, Inc., PROGRAM SURGE_STAT Users Manual, Version 1.1. November, 2009.

RAMPP, 2014 (Lettis Consultants International, Inc.), Region II Storm Surge Project - Joint Probability Analysis Of Hurricane and Extratropical Flood Hazards, FEMA TO HSFE02-09-J-001, 2013

Slinn, Don. November 20, 2010.Wave Setup Methodology for the Florida Panhandle Flood Study (Franklin, Wakulla, and Jefferson Counties, FL). University of Florida, Gainesville, Fla.

Slinn, Don, Draft Wave Setup Methodology for the Alabama-Florida Panhandle Flood Study, University of Florida, Gainesville, FL. Pending June 2013.

URS, Mississippi Coastal Analysis Project, Final Report: HMTAP Task Order 18, Coastal Documentation and Main Engineering Report, June 17, 2008.

Zundel, AK. 2000. Surface-water Modeling System reference manual," Brigham Young University, Environmental Modeling Research Laboratory, Provo, Ut.